

# Warm springs alter timing but not total growth of temperate deciduous trees

<https://doi.org/10.1038/s41586-022-05092-3>

Received: 18 November 2021

Accepted: 8 July 2022

Published online: 10 August 2022

 Check for updates

Cameron Dow<sup>1,2</sup>, Albert Y. Kim<sup>1,3</sup>, Loïc D'Orangeville<sup>4,5</sup>, Erika B. Gonzalez-Akre<sup>1</sup>, Ryan Helcoski<sup>1</sup>, Valentine Herrmann<sup>1</sup>, Grant L. Harley<sup>6</sup>, Justin T. Maxwell<sup>7</sup>, Ian R. McGregor<sup>1,8</sup>, William J. McShea<sup>1</sup>, Sean M. McMahon<sup>9,10</sup>, Neil Pederson<sup>4</sup>, Alan J. Tepley<sup>1,11,12</sup> & Kristina J. Anderson-Teixeira<sup>1,10</sup> 

As the climate changes, warmer spring temperatures are causing earlier leaf-out<sup>1–3</sup> and commencement of CO<sub>2</sub> uptake<sup>1,3</sup> in temperate deciduous forests, resulting in a tendency towards increased growing season length<sup>3</sup> and annual CO<sub>2</sub> uptake<sup>1,3–7</sup>. However, less is known about how spring temperatures affect tree stem growth<sup>8,9</sup>, which sequesters carbon in wood that has a long residence time in the ecosystem<sup>10,11</sup>. Here we show that warmer spring temperatures shifted stem diameter growth of deciduous trees earlier but had no consistent effect on peak growing season length, maximum growth rates, or annual growth, using dendrometer band measurements from 440 trees across two forests. The latter finding was confirmed on the centennial scale by 207 tree-ring chronologies from 108 forests across eastern North America, where annual ring width was far more sensitive to temperatures during the peak growing season than in the spring. These findings imply that any extra CO<sub>2</sub> uptake in years with warmer spring temperatures<sup>4,5</sup> does not significantly contribute to increased sequestration in long-lived woody stem biomass. Rather, contradicting projections from global carbon cycle models<sup>1,12</sup>, our empirical results imply that warming spring temperatures are unlikely to increase woody productivity enough to strengthen the long-term CO<sub>2</sub> sink of temperate deciduous forests.

In recent decades, tree growth in Earth's forests has more than offset losses from deforestation and other disturbances, such that a net forest CO<sub>2</sub> sink of approximately 1.6 Gt carbon per year offsets approximately 20% of anthropogenic emissions<sup>13</sup>, dramatically slowing the pace of atmospheric CO<sub>2</sub> accumulation and climate change. Of this important carbon sink, approximately 47% occurs in temperate forests<sup>13</sup>, with temperate deciduous forests sequestering more than 0.3 Gt carbon per year<sup>14</sup>. The future behaviour of this carbon sink will have an important yet uncertain role in influencing atmospheric CO<sub>2</sub> and climate change<sup>15–17</sup>.

In temperate deciduous forests, spring warming generally lengthens the period over which trees have photosynthetically active leaves<sup>1,3,18</sup> and that over which the ecosystem is a net CO<sub>2</sub> sink<sup>1,18</sup>. On the basis of these observations, current terrestrial ecosystem models represent warm spring temperatures and longer growing seasons as contributing positively to annual gross primary productivity (GPP) and net CO<sub>2</sub> uptake (that is, net ecosystem exchange (NEE))<sup>2,12,15</sup>. However, the long-term persistence of this extra carbon in the ecosystem, and the associated negative feedback to climate change<sup>1</sup>, will depend on the extent to which it is allocated to woody growth and therefore resides in the ecosystem for decades to centuries<sup>10,11</sup>, as opposed to being rapidly released

back to the atmosphere through respiration<sup>19,20</sup>. Model representation of carbon allocation to stem growth—or woody aboveground net primary productivity (ANPP<sub>woody</sub>) on the ecosystem level—does not capture known decoupling of stem growth from photosynthate production<sup>9,17,21</sup>. As a result, the consequences of rising spring temperatures on stem growth may not be accurately represented in models<sup>9,17</sup>. Understanding the sensitivity of ANPP<sub>woody</sub> to spring temperatures is central to predicting the future of the temperate deciduous forest carbon sink.

Most studies on tree stem growth responses to warmer spring temperatures have focused on boreal or temperate conifers, which tend to respond to warmer spring temperatures with an earlier start to growth<sup>22,23</sup> and increased annual growth in mesic climates<sup>24,25</sup>. By contrast, little evidence exists as to how stem growth and ANPP<sub>woody</sub> respond to warmer spring temperatures in deciduous forests<sup>8,9</sup>. Close coordination of budburst and initiation of xylogenesis<sup>9</sup> suggest that warm spring temperatures should shift the onset of growth earlier alongside observed advances in leaf phenology<sup>1–3</sup>. However, earlier initiation of growth would not necessarily translate to earlier, faster or greater stem growth; rather, stem growth is dependent on environmental conditions on hourly to daily timescales<sup>26,27</sup>, and

<sup>1</sup>Conservation Ecology Center, Smithsonian's National Zoo & Conservation Biology Institute, Front Royal, VA, USA. <sup>2</sup>Department of Forestry and Natural Resources, Purdue University, West Lafayette, IN, USA. <sup>3</sup>Statistical & Data Sciences, Smith College, Northampton, MA, USA. <sup>4</sup>Harvard Forest, Petersham, MA, USA. <sup>5</sup>Faculty of Forestry and Environmental Management, University of New Brunswick, Fredericton, New Brunswick, Canada. <sup>6</sup>Department of Earth and Spatial Sciences, University of Idaho, Moscow, ID, USA. <sup>7</sup>Department of Geography, Indiana University, Bloomington, IN, USA. <sup>8</sup>Center for Geospatial Analytics, North Carolina State University, Raleigh, NC, USA. <sup>9</sup>Smithsonian Environmental Research Center, Edgewater, MD, USA. <sup>10</sup>Forest Global Earth Observatory, Smithsonian Tropical Research Institute, Panama, Republic of Panama. <sup>11</sup>Canadian Forest Service, Northern Forestry Centre, Edmonton, Alberta, Canada. <sup>12</sup>Department of Forestry and Wildland Resources, Cal Poly Humboldt University, Arcata, CA, USA.  e-mail: teixeirak@si.edu

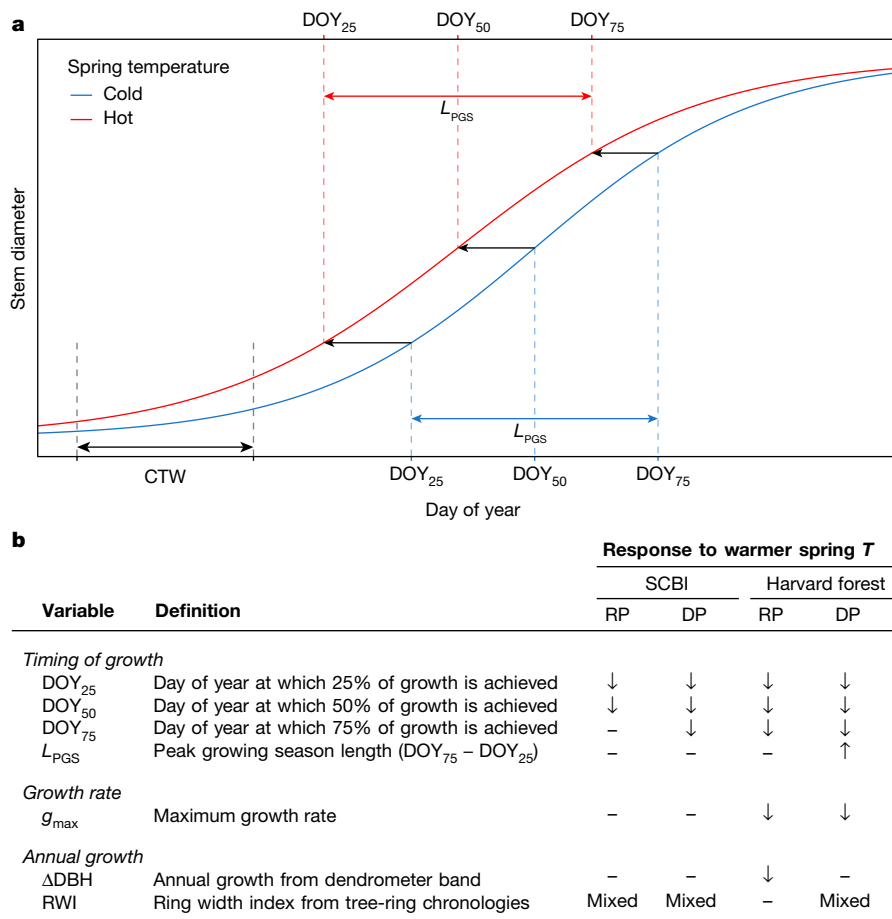


**Fig. 1 | Summary of temperate deciduous tree growth responses to warmer spring temperatures.** **a**, Schematic illustrating parameters of interest and summarizing predominant responses of each to warmer maximum temperatures during a critical temperature window (CTW), defined as the period with the strongest temperature control over DOY<sub>25</sub>. **b**, Variable definitions and summary of responses to warmer spring temperatures at two

temperate forests—SCBI and Harvard Forest—and for two groups of broadleaf deciduous species. The up and down arrows indicate increases and decreases, respectively, that are significant both statistically ( $P < 0.05$ ) and biologically (effect size  $> 3\%$  per °C); ‘-’ indicates no significant correlation; and ‘mixed’ indicates a mix of significant and non-significant correlations, often in different directions. DP, diffuse porous; RP, ring porous.

annual growth is more closely linked to conditions within the growing season than to growing season length<sup>28</sup>, GPP<sup>21</sup> or NEE<sup>21</sup>. Furthermore, growth of broadleaf deciduous trees may be sink-saturated<sup>17,29</sup>, such that longer growing seasons with more carbon fixation do not necessarily augment growth<sup>21,30,31</sup>. Tree-ring records, which can be used to examine annual growth but not growth seasonality, reveal that growth of temperate deciduous trees tends to be most sensitive to temperature or potential evapotranspiration between late spring and early summer<sup>32,33</sup>, with some evidence that warmer spring temperatures may have a modest positive effect on growth<sup>25,33</sup>. These observations do not necessarily align with the finding that warming spring temperatures increase annual forest CO<sub>2</sub> uptake in temperate deciduous forests<sup>1,18</sup>. Characterizing responses of stem growth to warming spring temperatures is critical to bridging this conceptual disconnect and understanding how forest biomass growth is likely to change as the climate warms.

Here, we evaluate how spring temperatures affect the timing, rates and annual increments of stem diameter growth of temperate deciduous trees across eastern North America. To test whether warmer spring temperatures advance the timing and extend the duration of stem diameter growth, we used dendrometer band measurements on 440 trees across two mid-latitude forests. To test whether warm spring temperatures consistently increased annual radial increments, we analysed 207 tree-ring chronologies from 108 forests.

## Dendrometer band analysis

Using dendrometer band measurements taken throughout multiple growing seasons at the Smithsonian Conservation Biology Institute (SCBI; VA, USA;  $n = 119$  trees from 2011 to 2020) and Harvard Forest (MA, USA;  $n = 321$  trees from 1998 to 2003), we fit a logistic growth model<sup>34</sup> to determine the days of year (DOYs) when 25%, 50% and 75% annual diameter growth were achieved (DOY<sub>25</sub>, DOY<sub>50</sub> and DOY<sub>75</sub>), the peak growing season length ( $L_{\text{PGS}} = \text{DOY}_{75} - \text{DOY}_{25}$ ), the maximum growth rate ( $g_{\max}$ ) and the total annual increment in diameter at breast height ( $\Delta\text{DBH}$ ; Fig. 1). This analysis was performed separately for ring-porous and diffuse-porous species (Extended Data Table 1), which differ in the seasonal timing of growth<sup>27,35</sup> (Extended Data Table 2 and Extended Data Fig. 1). These milestones in stem growth were compared with canopy foliage phenology (measured at the ecosystem level via remote sensing).

Both canopy foliage phenology and the timing of stem growth shifted earlier as spring temperatures increased (Fig. 2). We found a consistent effect of temperature ( $T_{\max}$  or  $T_{\min}$ ) throughout the spring, but the strongest effects on the timing of stem growth were found using  $T_{\max}$  during a critical temperature window (CTW). The CTW was identified by assessing the correlation between weekly  $T_{\max}$  and DOY<sub>25</sub> for all combinations of consecutive weeks from 1 January to mean DOY<sub>25</sub> for each xylem architecture–site combination (Extended Data

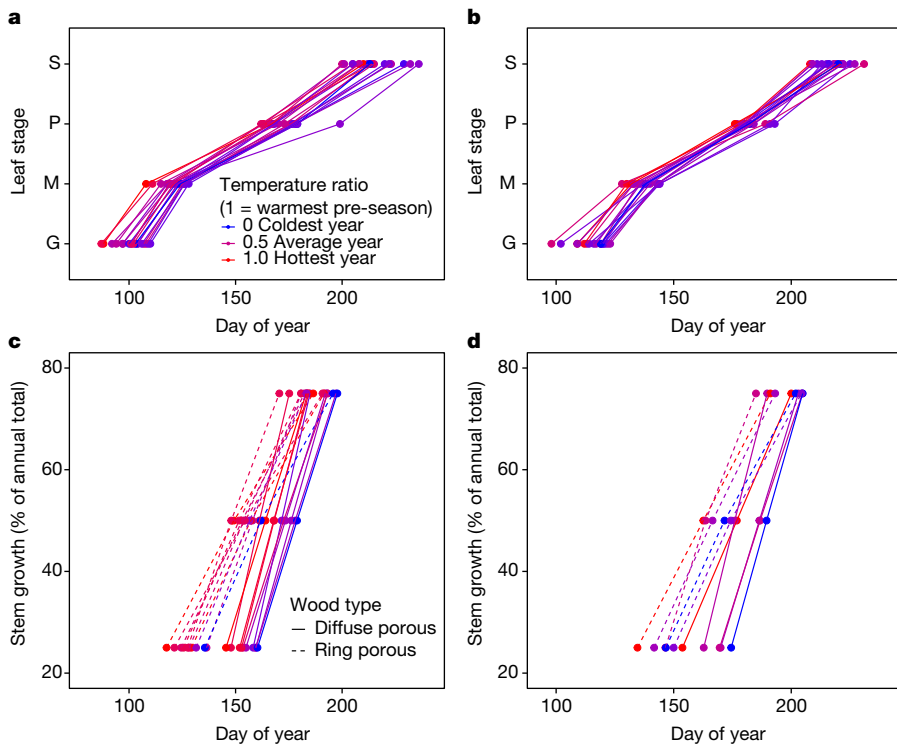


**Fig. 2 | Responses of foliage phenology and stem growth timing to spring temperatures at SCBI and Harvard Forest.** **a, b**, Ecosystem-level canopy foliage phenology from 2001 to 2018 at SCBI (**a**) and Harvard Forest (**b**), obtained from the MODIS Global Vegetation Phenology product (MCD12Q2.006) for a single pixel at the centre of each ForestGEO plot. G, greenup; M, mid-greenup; P, peak; S, senescence (that is, beginning of greendown). **c, d**, Dates at which stem growth milestones were achieved, on average, for sampled populations of ring-porous and diffuse-porous trees at SCBI (2011–2020; **c**) and Harvard Forest (1999–2003; **d**).

Mean DOY<sub>25</sub>, DOY<sub>50</sub> and DOY<sub>75</sub> were estimated using the Bayesian model visualized, with confidence intervals, in Extended Data Fig. 3. Mean  $T_{\max}$  was calculated for each xylem architecture–site combination over the respective CTW, then turned into a ratio and assigned a colour on a gradient in which the coldest year in the sample is blue and the warmest is red. Leaf phenology years are coloured according to the CTW  $T_{\max}$  of the porosity group containing the dominant canopy species at each site (diffuse porous at SCBI and ring porous at Harvard Forest).

Fig. 2). The CTW was defined as the weeks for which this correlation was strongest, and mean  $T_{\max}$  during this period (CTW  $T_{\max}$ ) was used as our independent variable.

For ring-porous and diffuse-porous species at both sites, warmer CTW  $T_{\max}$  resulted in earlier achievement of seasonal milestones. Consistent with findings from previous studies, leaf phenological milestones advanced at both sites (Fig. 2a,b and Extended Data Table 2), with greenup (DOY when the enhanced vegetation index (EVI2) first crossed 15% of the segment EVI2 amplitude) advancing 3.5 days per °C at SCBI ( $P = 0.016$ ) and 2.4 days per °C at Harvard Forest ( $P = 0.1$ ). Similarly, with the exception of ring-porous DOY<sub>75</sub> at SCBI, the stem growth milestones DOY<sub>25</sub>, DOY<sub>50</sub> and DOY<sub>75</sub> decreased with CTW  $T_{\max}$  (Figs. 1 and 2c,d and Extended Data Figs. 3 and 4). Specifically, DOY<sub>25</sub>, DOY<sub>50</sub> and DOY<sub>75</sub> advanced 0–1.7 days per °C for ring-porous species and 2.8–2.9 days per °C for diffuse-porous species at SCBI, and 10.3–12.3 days per °C for ring-porous species and 0.9–4.2 days per °C for diffuse-porous species at Harvard Forest (Extended Data Table 2).

Whereas the length of time between canopy greenup and senescence (that is, the day when greenness dropped below 90% of its peak) increased with the CTW  $T_{\max}$  of the porosity group containing the dominant canopy species at each site (diffuse porous at SCBI and ring porous at Harvard Forest; Fig. 2a,b), there was no consistent lengthening of  $L_{\text{pgs}}$  (Fig. 1 and Extended Data Figs. 3 and 4).

In contrast to the pronounced effects of CTW  $T_{\max}$  on the timing of growth, its effects on  $g_{\max}$  and  $\Delta\text{DBH}$  were inconsistent and usually weak (Fig. 1 and Extended Data Figs. 3 and 4). Specifically,  $g_{\max}$ , which occurred on average within 5 days of DOY<sub>50</sub>, displayed extremely

small negative changes (Harvard Forest) or changes in opposite directions (SCBI) in relationship to CTW  $T_{\max}$  for ring-porous and diffuse-porous species.  $\Delta\text{DBH}$  displayed a weak positive relationship (+0.003–0.008 cm per °C) with CTW  $T_{\max}$  at SCBI and a weak negative relationship (−0.02 to 0.003 cm per °C) at Harvard Forest (Extended Data Fig. 3).

### Tree-ring analysis

To understand how annual radial stem growth increments have responded to spring temperatures at the centennial scale, we analysed tree-ring chronologies of 12 species at SCBI<sup>33</sup> and four species at Harvard Forest (Extended Data Table 1), plus an additional 191 chronologies from 106 sites (Fig. 3, Extended Data Table 3 and Extended Data Fig. 5). In total, our analysis included 207 chronologies representing 24 broadleaf species at 108 sites distributed from Alabama (34.35° N latitude) to Michigan (45.56° N latitude) and spanning a 15 °C range in April  $T_{\max}$ . Across all chronologies, the standardized ring-width index (RWI) was significantly (95% confidence interval did not include 0) positively correlated with April  $T_{\max}$  for only 2% of chronologies: 1 of 142 ring-porous and 4 of 66 diffuse-porous species–site combinations (Extended Data Table 3). There were even fewer significant positive correlations with March and May  $T_{\max}$ : 0% and 1%, respectively (Extended Data Table 3). By contrast, RWI was frequently negatively correlated with  $T_{\max}$  during peak growing season months (May–August), with significant correlations for 52% (45 of 141 (May), 107 of 141 (June), 91 of 141 (July) and 53 of 141 (August)) and 46% (10 of 66 (May), 52 of 66 (June), 36 of 66 (July) and 23 of 66 (August)) of species–site–month

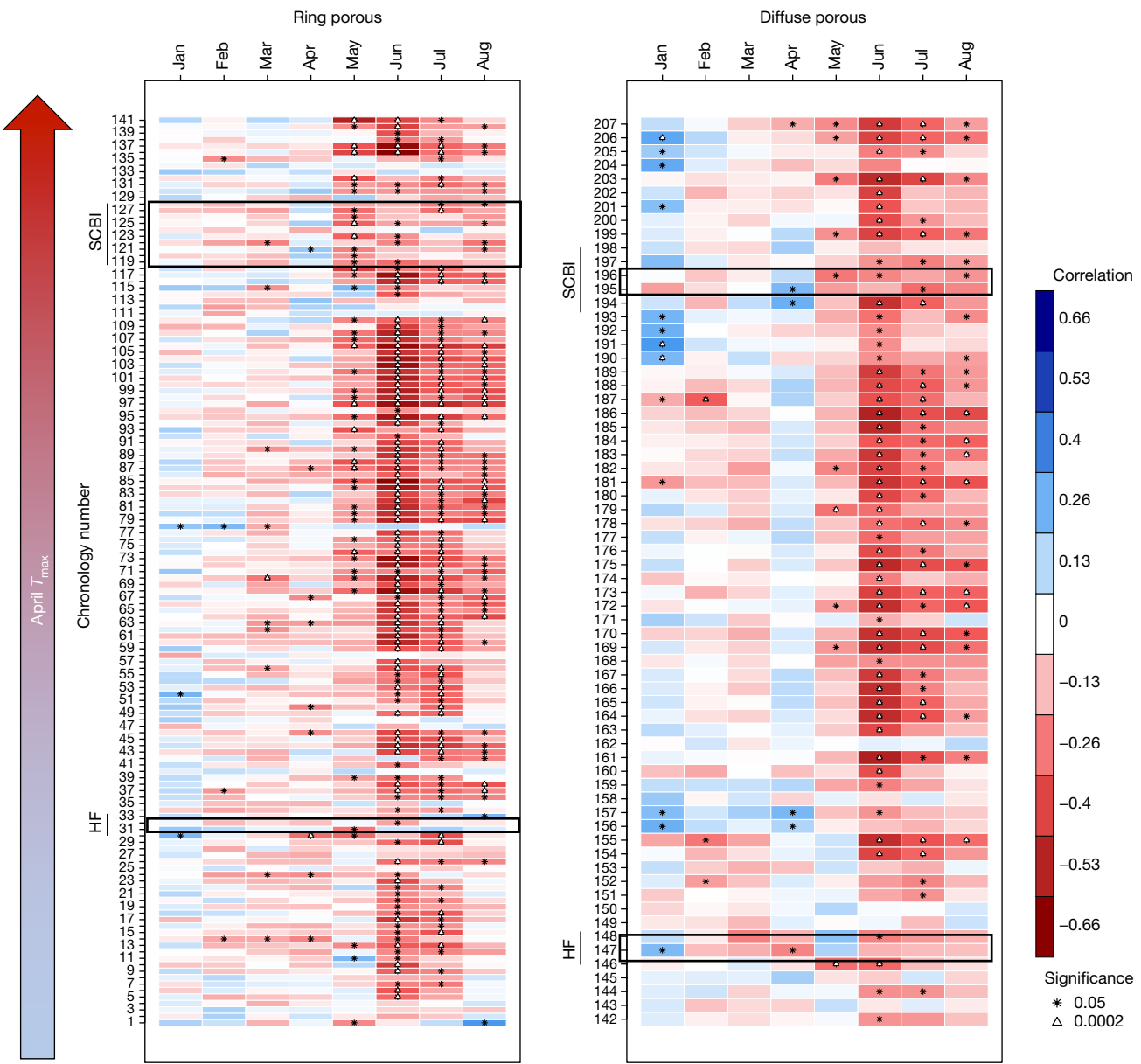


**Fig. 3 | Sensitivity of annual growth, as derived from tree rings, to monthly mean  $T_{\max}$ , for 207 chronologies from 108 sites across eastern North America.** Colours indicate the bootstrapped correlation between monthly  $T_{\max}$  and a dimensionless RWI derived from the multiple trees that form each chronology and emphasizing interannual variability associated with climate. Chronologies are grouped by xylem porosity and ordered by mean April  $T_{\max}$ .

Plots are annotated to highlight records from our two focal sites: SCBI and Harvard Forest (HF; Extended Data Table 1). Sites included are mapped in Extended Data Fig. 5, species analysed and numbers of significant correlations to  $T_{\max}$  are summarized in Extended Data Table 3, and chronology details are provided in Supplementary Table 1.

combinations for ring-porous and diffuse-porous species, respectively.  $T_{\min}$  generally exhibited weaker relationships to annual growth than  $T_{\max}$ , with few significant correlations between spring  $T_{\min}$  and RWI (Extended Data Fig. 6).

To test whether warm spring temperatures might result in storage of non-structural carbohydrates that would augment growth the following year<sup>36</sup>, we extended the analysis to examine correlations between RWI and  $T_{\max}$  in the previous year (Extended Data Fig. 7). This revealed little effect of previous spring temperatures on annual growth, with significant positive correlations of RWI to previous March or April  $T_{\max}$  for 5 of 142 ring-porous chronologies and to previous April or May  $T_{\max}$  for 7 of 66 diffuse-porous chronologies.

To test whether there may be an enhancement of growth by warmer spring temperatures that was offset by the negative effect of high

summer temperatures, we tested for the joint effects of April and June–July  $T_{\max}$  on RWI. Results were qualitatively similar to the univariate correlations (Fig. 3), with significant ( $P \leq 0.05$ ) positive correlations to April  $T_{\max}$  for only 4% of chronologies and significant negative correlations with June–July  $T_{\max}$  for 77% of chronologies (Extended Data Table 3).

## Discussion

Together, our results demonstrate that warmer spring temperatures in the temperate deciduous forests of eastern North America advance the timing of stem diameter growth but have little effect on annual increments (Figs. 1–3). The observed advance in stem growth under warmer spring temperatures parallels advances observed for canopy foliage phenology<sup>1,3</sup> (Fig. 2a,b) and NEE<sup>1,3</sup>. However, inconsistent with

# Article

the concept that an earlier start to growth would increase ANPP<sub>woody</sub>, we demonstrate that warmer spring temperatures either hasten the deceleration of stem expansion or otherwise fail to translate extended growing seasons into biologically significant increases in stem growth (Fig. 1), and thereby have negligible effect on total annual growth for most species and locations (Fig. 3). Our observations suggest that the deceleration of stem expansion, which occurs in mid-summer near the time of peak canopy greenness<sup>3,28</sup> (Extended Data Fig. 1), is driven by cues other than photosynthate limitation, such as water stress<sup>21,26,28</sup>, nutrient limitation<sup>37</sup>, day length<sup>28</sup> or sink saturation<sup>21,29</sup>. This adds to a growing body of evidence for a sink limitation of stem growth<sup>17,21,31</sup>, in which global change factors known to enhance photosynthesis, such as longer growing seasons or elevated levels of CO<sub>2</sub>, do not cause a corresponding increase in stem growth<sup>19,28</sup>.

Combined with widespread observations that warming spring temperatures tend to lengthen the season of CO<sub>2</sub> uptake<sup>3,18</sup> and increase net annual CO<sub>2</sub> uptake<sup>1,3–7</sup>, our findings imply a lengthening of the period from peak stem growth to the cessation of CO<sub>2</sub> uptake by the ecosystem and an increase in carbon allocated to functions other than stem expansion in the current or following year. It remains theoretically possible that warm spring temperatures could augment ANPP<sub>woody</sub>, which, although routinely calculated based on stem growth, can be partially decoupled from it through differences in wood density or carbon content<sup>21</sup>. Extra carbon fixed in years with warm spring temperatures could potentially be allocated to the formation of more carbon-dense wood, either through enhanced cell wall thickening (a process that lags behind stem expansion<sup>38</sup>) or to a higher ratio of high-density latewood to lower-density earlywood. However, existing evidence indicates that vessel features are most strongly controlled by summer drought stress in the previous (earlywood) or current (latewood) year, whereas warm spring temperatures have a neutral or negative effect on the width of latewood<sup>39–41</sup>. Thus, it is unlikely that warm spring temperatures have a positive effect on total carbon content of annual rings or ANPP<sub>woody</sub>.

The fate of any additional carbon fixed during years with warm spring temperatures remains unresolved, but possible destinations—including respiration, non-structural carbohydrate storage and production of foliage, reproductive structures, roots<sup>30</sup> or root exudates—generally have shorter residence times than woody growth. Indeed, when GPP of a mature forest was increased through experimental enrichment of CO<sub>2</sub>, ANPP<sub>woody</sub> remained unchanged, whereas additional carbon was released back to the atmosphere on relatively short timescales through enhanced respiration<sup>19</sup>. Consistent with this, it has been observed that carbon gains from an earlier spring can be offset through autumn or winter respiration<sup>20</sup>, although even the carbon in shorter-lived pools would often be carried over into the following year<sup>42</sup>. Thus, observed augmentation of NEE by warm spring temperatures<sup>1,6,7</sup> is likely to be compensated by increased respiration in subsequent years.

It is possible that as spring warming continues, forests will adjust to directional changes in growing season length with an enhancement of ANPP<sub>woody</sub>. Across latitudinal gradients, warmer spring temperatures are associated with earlier leaf-out<sup>43</sup> and longer growing seasons, which in turn are correlated with greater tree growth<sup>44</sup>, ANPP<sub>woody</sub> (ref. <sup>45</sup>) and NEE<sup>46</sup>. Thus, warming spring temperatures are likely to increase the biophysical potential for annual tree growth. If extra photosynthate made available through a growing difference between GPP and ANPP<sub>woody</sub> is allocated to functions that relieve limitations on woody growth—for example, by enhancing nutrient and water acquisition through enhanced allocation to roots<sup>30,47</sup>—it is possible that warming spring temperatures could ultimately increase ANPP<sub>woody</sub> through indirect mechanisms. Understanding how warming spring temperatures are influencing carbon allocation within ecosystems remains a key outstanding question.

Regardless of the influence of spring temperatures on carbon cycling within the ecosystem, our results clearly demonstrate that the dominant effects of temperature on deciduous tree growth occur not in the spring, but during the peak growing season of the current

or sometimes previous year (Fig. 3 and Extended Data Fig. 7), when increased atmospheric demand associated with high temperatures can limit both leaf-level gas exchange and stem growth<sup>21,26,28,48</sup>. Indeed, the timing of peak growth in June and July (Extended Data Table 2 and Extended Data Fig. 1) coincides with the timing of the greatest sensitivity of annual growth to T<sub>max</sub> (Fig. 3 and Extended Data Table 3). This finding is consistent with numerous tree-ring studies demonstrating strong sensitivity of growth to drought stress or high temperatures during the peak growing season<sup>24,32,33,44</sup>. Warm spring temperatures may also amplify summer drought stress in some times and places, effectively cancelling out any positive effects of an extended growing period<sup>4,49,50</sup>. Although such an interaction was unlikely to have had a major role within the scope of our dendrometer band study, given relatively mesic conditions and lack of significant correlation between spring temperatures and summer drought stress (see Methods), our tree-ring analysis does reveal a higher frequency of negative than positive correlations of annual growth to spring temperatures, particularly for ring-porous species in cooler climates (Fig. 3 and Extended Data Table 3). Thus, warm spring temperatures can have a net negative effect on growth, particularly when water is limiting<sup>25</sup>.

As spring temperatures become increasingly warmer, growing seasons will start earlier. However, barring rapid acclimation of temperate deciduous forests to the warming conditions, advancement in the timing of stem growth (Fig. 1) is unlikely to provide a sustained augmentation of carbon sequestration in woody biomass and ensuant negative climate change feedback that is anticipated in most climate forecasting models<sup>1,2,12,31</sup>. Rather, the dominant effect of rising temperatures on temperate deciduous forest woody productivity will be a negative effect of high summer temperatures<sup>15</sup> (Fig. 3), which constitutes a positive feedback to climate change.

## Online content

Any methods, additional references, Nature Research reporting summaries, source data, extended data, supplementary information, acknowledgements, peer review information; details of author contributions and competing interests; and statements of data and code availability are available at <https://doi.org/10.1038/s41586-022-05092-3>.

- Keenan, T. F. et al. Net carbon uptake has increased through warming-induced changes in temperate forest phenology. *Nat. Clim. Chang.* **4**, 598–604 (2014).
- Buermann, W. et al. Widespread seasonal compensation effects of spring warming on northern plant productivity. *Nature* **562**, 110–114 (2018).
- Finzi, A. C. et al. Carbon budget of the Harvard Forest Long-Term Ecological Research site: pattern, process, and response to global change. *Ecol. Monogr.* **90**, e01423 (2020).
- Keeling, C. D., Chin, J. F. S. & Whorf, T. P. Increased activity of northern vegetation inferred from atmospheric CO<sub>2</sub> measurements. *Nature* **382**, 146–149 (1996).
- Dragon, D. et al. Evidence of increased net ecosystem productivity associated with a longer vegetated season in a deciduous forest in south-central Indiana, USA. *Glob. Chang. Biol.* **17**, 886–897 (2011).
- Zhou, S. et al. Explaining inter-annual variability of gross primary productivity from plant phenology and physiology. *Agric. For. Meteorol.* **226–227**, 246–256 (2016).
- Fu, Z. et al. Maximum carbon uptake rate dominates the interannual variability of global net ecosystem exchange. *Glob. Chang. Biol.* **25**, 3381–3394 (2019).
- Savage, J. A. & Chuine, I. Coordination of spring vascular and organ phenology in deciduous angiosperms growing in seasonally cold climates. *New Phytol.* **230**, 1700–1715 (2021).
- Delpierre, N. et al. Temperate and boreal forest tree phenology: from organ-scale processes to terrestrial ecosystem models. *Ann. For. Sci.* **73**, 5–25 (2016).
- Xue, B.-L. et al. Global patterns of woody residence time and its influence on model simulation of aboveground biomass. *Global Biogeochem. Cycles* **31**, 821–835 (2017).
- Russell, M. B. et al. Residence times and decay rates of downed woody debris biomass/carbon in eastern US forests. *Ecosystems* **17**, 765–777 (2014).
- Richardson, A. D. et al. Terrestrial biosphere models need better representation of vegetation phenology: results from the North American Carbon Program Site Synthesis. *Glob. Chang. Biol.* **18**, 566–584 (2012).
- Harris, N. L. et al. Global maps of twenty-first century forest carbon fluxes. *Nat. Clim. Chang.* **11**, 234–240 (2021).
- Pugh, T. A. M. et al. Role of forest regrowth in global carbon sink dynamics. *Proc. Natl Acad. Sci. USA* **116**, 4382–4387 (2019).
- Ahlström, A., Schurgers, G., Arneth, A. & Smith, B. Robustness and uncertainty in terrestrial ecosystem carbon response to CMIP5 climate change projections. *Environ. Res. Lett.* **7**, 044008 (2012).

16. Friedlingstein, P. et al. Global carbon budget 2020. *Earth Syst. Sci. Data* **12**, 3269–3340 (2020).
17. Fatichi, S., Leuzinger, S. & Körner, C. Moving beyond photosynthesis: from carbon source to sink-driven vegetation modeling. *New Phytol.* **201**, 1086–1095 (2014).
18. Lu, X. & Keenan, T. F. No evidence for a negative effect of growing season photosynthesis on leaf senescence timing. *Glob. Chang. Biol.* **28**, 3083–3093 (2022).
19. Jiang, M. et al. The fate of carbon in a mature forest under carbon dioxide enrichment. *Nature* **580**, 227–231 (2020).
20. Oishi, A. C. et al. Warmer temperatures reduce net carbon uptake, but do not affect water use, in a mature southern Appalachian forest. *Agric. For. Meteorol.* **252**, 269–282 (2018).
21. Delpierre, N., Berveiller, D., Granda, E. & Dufrêne, E. Wood phenology, not carbon input, controls the interannual variability of wood growth in a temperate oak forest. *New Phytol.* **210**, 459–470 (2016).
22. Huang, J.-G. et al. Photoperiod and temperature as dominant environmental drivers triggering secondary growth resumption in Northern Hemisphere conifers. *Proc. Natl Acad. Sci. USA* **117**, 20645–20652 (2020).
23. Rossi, S. et al. Critical temperatures for xylogenesis in conifers of cold climates. *Global Ecol. Biogeogr.* **17**, 696–707 (2008).
24. Babst, F. et al. Twentieth century redistribution in climatic drivers of global tree growth. *Sci. Adv.* **5**, eaat4313 (2019).
25. Gao, S. et al. An earlier start of the thermal growing season enhances tree growth in cold humid areas but not in dry areas. *Nat. Ecol. Evol.* **6**, 397–404 (2022).
26. Zweifel, R. et al. Why trees grow at night. *New Phytol.* **231**, 2174–2185 (2021).
27. Turnajer, J., Scharnweber, T., Smiljanic, M. & Wilmking, M. Limitation by vapour pressure deficit shapes different intra-annual growth patterns of diffuse- and ring-porous temperate broadleaves. *New Phytol.* **233**, 2429–2441 (2022).
28. Etzold, S. et al. Number of growth days and not length of the growth period determines radial stem growth of temperate trees. *Ecol. Lett.* **25**, 427–439 (2022).
29. Zani, D., Crowther, T. W., Mo, L., Renner, S. S. & Zohner, C. M. Increased growing-season productivity drives earlier autumn leaf senescence in temperate trees. *Science* **370**, 1066–1071 (2020).
30. Zohner, C. M., Renner, S. S., Sebald, V. & Crowther, T. W. How changes in spring and autumn phenology translate into growth—experimental evidence of asymmetric effects. *J. Ecol.* **109**, 2717–2728 (2021).
31. Cabon, A. et al. Cross-biome synthesis of source versus sink limits to tree growth. *Science* **376**, 758–761 (2022).
32. D'Orangeville, L. et al. Drought timing and local climate determine the sensitivity of eastern temperate forests to drought. *Glob. Chang. Biol.* **24**, 2339–2351 (2018).
33. Helcoski, R. et al. Growing season moisture drives interannual variation in woody productivity of a temperate deciduous forest. *New Phytol.* **223**, 1204–1216 (2019).
34. McMahon, S. M. & Parker, G. G. A general model of intra-annual tree growth using dendrometer bands. *Ecol. Evol.* **5**, 243–254 (2015).
35. D'Orangeville, L. et al. Peak radial growth of diffuse-porous species occurs during periods of lower water availability than for ring-porous and coniferous trees. *Tree Physiol.* **42**, 304–316 (2022).
36. Richardson, A. D. et al. Seasonal dynamics and age of stemwood nonstructural carbohydrates in temperate forest trees. *New Phytol.* **197**, 850–861 (2013).
37. Elmore, A. J., Nelson, D. M. & Craine, J. M. Earlier springs are causing reduced nitrogen availability in North American eastern deciduous forests. *Nat. Plants* **2**, 16133 (2016).
38. Cuny, H. E. et al. Woody biomass production lags stem-girth increase by over one month in coniferous forests. *Nat. Plants* **1**, 15160 (2015).
39. Tardif, J. C. & Conciatori, F. Influence of climate on tree rings and vessel features in red oak and white oak growing near their northern distribution limit, southwestern Quebec, Canada. *Can. J. For. Res.* **36**, 2317–2330 (2006).
40. Roibu, C.-C. et al. The climatic response of tree ring width components of ash (*Fraxinus excelsior* L.) and common oak (*Quercus robur* L.) from eastern Europe. *Forests* **11**, 600 (2020).
41. Kern, Z. et al. Multiple tree-ring proxies (earlywood width, latewood width and δ<sup>13</sup>C) from pedunculate oak (*Quercus robur* L.), Hungary. *Quat. Int.* **293**, 257–267 (2013).
42. Trumbore, S., Gaudinski, J. B., Hanson, P. J. & Southon, J. R. Quantifying ecosystem-atmosphere carbon exchange with a <sup>14</sup>C label. *Eos. Trans. Am. Geophys. Union* **83**, 265–268 (2002).
43. Del Mar Delgado, M. et al. Differences in spatial versus temporal reaction norms for spring and autumn phenological events. *Proc. Natl Acad. Sci. USA* **117**, 31249–31258 (2020).
44. Anderson-Teixeira, K. J. et al. Joint effects of climate, tree size, and year on annual tree growth derived from tree-ring records of ten globally distributed forests. *Glob. Chang. Biol.* **28**, 245–266 (2022).
45. Banbury Morgan, R. et al. Global patterns of forest autotrophic carbon fluxes. *Glob. Chang. Biol.* **27**, 2840–2855 (2021).
46. Churkina, G., Schimel, D., Braswell, B. H. & Xiao, X. Spatial analysis of growing season length control over net ecosystem exchange. *Glob. Chang. Biol.* **11**, 1777–1787 (2005).
47. Liu, H. et al. Phenological mismatches between above- and belowground plant responses to climate warming. *Nat. Clim. Chang.* **12**, 97–102 (2022).
48. Novick, K. A. et al. The increasing importance of atmospheric demand for ecosystem water and carbon fluxes. *Nat. Clim. Chang.* **6**, 1023–1027 (2016).
49. Zhang, J. et al. Drought limits wood production of *Juniperus przewalskii* even as growing seasons lengthens in a cold and arid environment. *CATENA* **196**, 104936 (2021).
50. Lian, X. et al. Summer soil drying exacerbated by earlier spring greening of northern vegetation. *Sci. Adv.* **6**, eaax0255 (2022).

**Publisher's note** Springer Nature remains neutral with regard to jurisdictional claims in published maps and institutional affiliations.

© This is a U.S. Government work and not under copyright protection in the US; foreign copyright protection may apply 2022

## Methods

### Dendrometer band analysis

Dendrometer band measurements were collected at SCBI<sup>51</sup> and Harvard Forest<sup>3,35</sup>, both part of the Forest Global Earth Observatory (ForestGEO)<sup>52,53</sup>. SCBI (38.8935° N, 78.1454° W; elevation 273–338 metres above sea level (m.a.s.l.)) is located in the Blue Ridge Mountains at the northern end of Shenandoah National Park, 5 km south of Front Royal, VA, USA. The forest is secondary and mixed age, having established in the mid-nineteenth century after conversion from agricultural fields<sup>51</sup>. Dominant canopy species within the 25.6 ha ForestGEO plot include tulip poplar (*Liriodendron tulipifera* L.), oaks (*Quercus* spp.) and hickories (*Carya* spp.)<sup>33</sup>. The climate is humid temperate, with the 1950–2019 mean annual precipitation of 1,018 mm and temperatures averaging 1 °C in January and 24 °C in July<sup>44</sup>. Within the study period for the dendrometer band analysis (2011–2019), spring temperatures (March and April  $T_{\max}$ ; source: CRU v.4.04 (ref. <sup>54</sup>)) and the summer standardized precipitation evapotranspiration index (SPEI)<sup>55</sup> values (4-month value of August) were similar to the average climate before the study period (1970–2010). Specifically, average spring  $T_{\max}$  was  $16.9 \pm 1.4$  °C (mean  $\pm 1$  s.d.) before the study period (range: 14.1–19.9) and  $17.6 \pm 1.7$  °C (range: 15.6–20) during the study period, whereas the summer SPEI was  $-0.06 \pm 1.02$  (range: -1.7 to 2.4) before the study period and  $0.5 \pm 0.8$  (range: -0.8 to 1.6) during.

Harvard Forest (42.5388° N, 72.1755° W; elevation 340–368 m.a.s.l.) is located near the central Massachusetts town of Petersham. The forest is secondary and mixed age, having re-established around the beginning of the twentieth century following agricultural use and significant hurricane damage in 1938. Dominant species within the 35 ha ForestGEO plot are hemlock (*Tsuga canadensis* (L.) Carrière), oak (*Quercus* spp.) and red maple (*Acer rubrum* L.). The climate is temperate continental, with the 1950–2019 mean annual precipitation of 1,104 mm and temperatures averaging -5 °C in January and 22 °C in July<sup>44</sup>. Within the study period for the dendrometer band analysis (1999–2003), spring temperatures (March and April  $T_{\max}$ ; source: CRU v.4.04 (ref. <sup>54</sup>)) and summer SPEI values (4-month value of August) were similar to the average climate before the study period (1970–1998). Specifically, average spring  $T_{\max}$  was  $10.9 \pm 1.5$  °C before the study period (range: 8.0–13.2) and  $11.2 \pm 1.0$  °C (range: 10.1–12.2) during the study period, whereas the summer SPEI was  $0.1 \pm 0.9$  (range: -1.8 to 1.7) before the study period and  $0.2 \pm 0.9$  (range: -1.0 to 1.1) during. The driest summer during the study period (1999) had the fifth lowest SPEI value (-1.0) in the period 1970–2003, with precipitation of 52 mm per month in June–August compared to average monthly precipitation of 100 mm or more<sup>35</sup>.

Metal dendrometer bands were installed on 941 trees within the SCBI and Harvard Forest ForestGEO plots. Bands were placed on dominant species, including two diffuse and two ring-porous species at SCBI and eight diffuse and three ring-porous species at Harvard Forest (Extended Data Table 1). Although we do not estimate the ages of the trees in our sample, bands at both sites were placed on individuals of differing sizes in an attempt to measure trees across a range of ages. Bands were measured with a digital calliper approximately every 1–2 weeks within the growing season from 2011 to 2020 at SCBI and 1998 to 2003 at Harvard Forest. The number of bands measured at each site fluctuated slightly as trees were added or dropped from the census (for example, because of tree mortality). Across years, the number of bands sampled averaged 129 (range: 91–138) at SCBI and 717 (range: 700–755) at Harvard Forest.

Measurements were timed to begin before the beginning of spring growth and to continue through the cessation of growth in the fall. At SCBI, the median start date was 14 April, which was adjusted forward when early leaf-out of understory vegetation was observed, with the earliest start date being 30 March (in 2020). Measurements were continued through to fall leaf senescence, with the median end date being 17 October and the latest end date being 26 November (in 2012). At Harvard Forest, all measurements from 1998 were dropped because

of a late start date (26 May). Among the remaining years, the median start date was 21 April and the median end date of 27 October 1999 was an anomalous year in which initial measurements were taken on 5 January, but were not taken again until 15 April. The latest end date was 11 November 2002. In our analysis, each band year was treated independently, with no data overlap from one year to the next.

The raw dendrometer band data were screened to remove records or entire tree-years that were inappropriate for our analysis because of reduced reliability of predicted growth in the modelled curves. Specifically, we removed tree-years with small or negligible total growth ( $\Delta\text{DBH} \leq 0.005$  cm; SCBI = 26, Harvard Forest = 253) and tree-years in which the first intra-annual measurement was later than the first spring survey (trees that were missed in the initial census; SCBI = 22, Harvard Forest = 8). In total, this process removed 309 of the 2,701 available tree-year records for 2011–2020 at SCBI and 1999–2003 at Harvard Forest.

We fit a five-parameter logistic growth model<sup>34</sup> to dendrometer band data from each tree-year to define stem growth milestones and growth rates (Fig. 1). In particular, we modelled the observed DBH on a given DOY (that is, Julian days) as:

$$\text{DBH} = L + \frac{K - L}{1 + 1/\theta \cdot \exp[-r(\text{DOY} - \text{DOY}_{\text{ip}})/\theta]}^{\theta}$$

Here,  $L$  and  $K$  are lower and upper asymptotes of the model.  $\text{DOY}_{\text{ip}}$  is the DOY during which the inflection point in growth rate occurs,  $r$  shapes the slope of the curve at the inflection point, and  $\theta$  is a tuning parameter controlling the slope of the curve towards the upper asymptote. This allows an asymmetric fit to the data, in which the onset of growth can be estimated independent of the cessation of growth. When  $\theta = 1$ ,  $\text{g}_{\max}$  occurs on  $\text{DOY}_{\text{ip}}$ . The model outputs two additional variables,  $a$  and  $b$ , which represent the beginning and end DBH in each model year and are constrained by the first and last dendrometer band measurements. The model was fit in R v4.0 using the functions developed in the Rdendrom package<sup>34</sup>. These functions take the time series of manual dendrometer band measurements and return maximum-likelihood-optimized values of the above five parameters that best predict DBH for each DOY. An advantage of this approach is that short-term shrinkage and swelling associated with rain events<sup>34,56</sup> and measurement errors show up as residual variation and do not unduly influence the parameters of interest. Having fit the model for each band year of data, we then modelled DBH using these optimal parameter values in our logistic growth model and extracted the intra-annual growth variables of interest (Fig. 1).

After fitting the growth model, we removed tree-years with poor fits. Models were judged to be poorly fit if modelled growth parameters were outliers, which were commonly indicative of unrealistic fits (for example, growth occurring outside the growing season or over a very short period) and underlain by very slow tree growth or poor data records that passed the initial screening (described above). Modelled fits for tree-years were removed under two conditions: (1)  $\text{g}_{\max}$  was 2.5 or more standard deviations away from the mean for each site–xylem architecture group combination (SCBI = 3, Harvard Forest = 11), and (2) timing variables ( $\text{DOY}_{\text{ip}}$ ,  $\text{DOY}_{25}$ ,  $\text{DOY}_{50}$  and  $\text{DOY}_{75}$ ) were 2.5 or more standard deviations away from the means for their site, xylem architecture group and year (SCBI = 74, Harvard Forest = 101). In total, this process removed 189 of the 2,392 tree-year records deemed appropriate for analysis, leaving a total of 2,203 tree-years included in the final analysis (Extended Data Table 1). At both sites, the tree-years removed through this method were proportional to the original sample size, indicating that no species or size class was disproportionately removed compared with others. This process was repeated using 2 and 3 standard deviations as the cut-off for defining outliers, yielding qualitatively similar results.

Canopy foliage phenology data for the years 2001–2018 were extracted for SCBI and Harvard Forest from the MCD12Q2 V6 Land

Cover Dynamics product (that is, MODIS Global Vegetation Phenology product)<sup>57</sup> via Google Earth Engine. For each year at each site, we extracted data from the pixel (500-m resolution) containing the centre of each forest plot. Using the daily MODIS 2-band EVI2 data, the product yields the timing of phenometrics (vegetation phenology) over each year, including timing of greenup, mid-greenup, peak and senescence, as used in this study. Data points were included in the analysis if they were flagged as ‘good’ or ‘best’ quality.

For the dendrometer band and leaf phenology analyses, climate data corresponding to the measurement periods were obtained from local weather stations at each focal site. For SCBI, weather data were obtained from a meteorological tower adjacent to the ForestGEO plot, via the ForestGEO Climate Data Portal v1.0 (<https://forestgeo.github.io/Climate/>)<sup>58</sup>. The R package climpact (see [www.climpact-sci.org](http://www.climpact-sci.org))<sup>59</sup> was used to plot temperatures for visual inspection and to identify readings that were more than 3 standard deviations away from yearly means, which were labelled as outliers and removed from the dataset. Gaps in the SCBI meteorological tower data were subsequently filled using temperature readings obtained from a National Center for Environmental Information (NCEI) weather station located in Front Royal, VA, USA (<https://www.ncdc.noaa.gov/cdo-web/datasets/GHCND/stations/GHCND:USC00443229/detail>). Daily temperature records for Harvard Forest, which had already been gap-filled on the basis of other local records, were obtained from the Harvard Forest weather station<sup>60,61</sup>. For each site, we used records of daily maximum ( $T_{\max}$ ) and minimum ( $T_{\min}$ ) temperatures. SPEI<sup>55</sup> values were obtained from the ForestGEO Climate Data Portal v1.0 (<https://forestgeo.github.io/Climate/>)<sup>55,58,62</sup>.

The CTW (Fig. 1), defined as the period over which  $T_{\max}$  was most strongly correlated with DOY<sub>25</sub>, was determined using the R package climwin<sup>63</sup>. This package tests the correlation between one or more predictor climate variable and a biological outcome variable over all consecutive time windows within a specified timeframe. It does so by reporting the correlation and  $\Delta\text{AICc}$ , the difference in Akaike information criterion corrected for small sample size relative to a null model for each window. Here, we tested for correlation between temperature predictor variables ( $T_{\max}$  and  $T_{\min}$ ) and biological outcome variable DOY<sub>25</sub> over the timeframe from 1 January to the mean DOY<sub>25</sub> for the species group (by xylem porosity) and site (Extended Data Table 2). The time period yielding the lowest  $\Delta\text{AICc}$  was selected as the CTW. To avoid spurious correlations that could occur using temperature data at the daily resolution, we ran this analysis with weekly resolution, using temperatures averaged over weekly time periods. Because  $T_{\max}$  proved to have a generally stronger influence over DOY<sub>25</sub> and other growth parameters, we focused on this variable in our ultimate model, as opposed to  $T_{\min}$ . We defined CTW for DOY<sub>25</sub>, as opposed to other parameters describing the timing of growth, because spring temperatures should have the most direct influence on this variable.

To ensure that patterns were robust under an alternative definition of CTW, and to parallel the monthly time windows used in our tree-ring analysis (detailed below; Fig. 3 and Extended Data Figs. 6 and 7), we also ran analyses in which we fixed the CTW identified by climwin to be the month with the most days in the CTW (Extended Data Table 2) for each critical window. The months identified were March and April for ring-porous and diffuse-porous species at SCBI, respectively, and April and May for ring-porous and diffuse-porous species at Harvard Forest, respectively.

Correlation between the dendrometer band-derived growth parameters (DOY<sub>25</sub>, DOY<sub>50</sub>, DOY<sub>75</sub>,  $L_{\text{pgs}}$ ,  $g_{\max}$  and  $\Delta\text{DBH}$ ; Fig. 1) and CTW  $T_{\max}$  (at weekly or monthly resolution, as described above) were assessed using a linear mixed model in a hierarchical Bayesian framework. Analyses were run for both  $T_{\max}$  and  $T_{\min}$ , with qualitatively similar results, but we present only results for  $T_{\max}$ , which had an overall stronger correlation with growth parameters. Mixed-effect models were used to test the response of growth parameters to fixed effects of xylem porosity and mean  $T_{\max}$  (or  $T_{\min}$ ) during the CTW, along with random effects of species

and of individual tree. We ran separate models for each site, and for the response of all growth parameters to  $T_{\max}$  (or  $T_{\min}$ ). This mixed-effect model was run within a hierarchical Bayesian framework and fit using the rstanarm version 2.21.3 R interface to the Stan programming language<sup>64,65</sup>. In all cases, unless otherwise specified, all prior distributions were set to be the weakly informative defaults.

To rule out the possibility that observed patterns were strongly influenced by summer drought, we examined the relationship between spring temperatures and summer SPEI indices. Linear models were run with 4-month, 6-month and 12-month SPEI values of June, July and August versus April  $T_{\max}$  to determine whether warm spring temperatures were associated with greater summer drought stress in our dataset. No significant correlations were found (all  $P > 0.05$ ).

### Tree-ring analysis

We analysed tree-ring records for 108 sites, including our focal sites. All cores had been previously collected, cross-dated and measured using standard collection and processing methodologies<sup>66,67</sup>.

Dominant tree species were cored at both SCBI<sup>33,51</sup> and Harvard Forest<sup>3,68,69</sup> following sampling designs that covered a broad range of DBH. We analysed records for the ring-porous and diffuse-porous species at each site (Extended Data Table 1), but excluded semi-ring-porous species (for example, *Juglans nigra* L. at SCBI) and conifers (for example, *Tsuga canadensis* at Harvard Forest). We studied a total of 976 cores, which included 12 species at SCBI and four species at Harvard Forest (Extended Data Table 1).

The tree-ring records from our focal sites were complemented with a much larger collection spanning 106 deciduous and mixed forest sites in eastern North America<sup>32,70,71</sup>. For the majority of sampled populations (that is, site–species combinations), sampling focused on canopy trees (typically more than 20 trees per population)<sup>32,70,71</sup>, whereas approximately 15% of the total 207 chronologies came from plot-level collections in which trees above a certain diameter (typically 10-cm DBH) were censused and cored<sup>33,69</sup>. Again, analyses were limited to broadleaf deciduous species with clearly defined xylem porosity (that is, excluding semi-ring porous).

For each species–site combination, we converted tree-ring records into the dimensionless RWI to emphasize interannual variability associated with climate<sup>72</sup>. A two-thirds  $n$  spline was applied to each core using ARSTAN V49\_1b to produce standardized ring-width series;  $n$  is the number of years in each series<sup>72,73</sup>. An adaptive power transformation, a process that also stabilizes the variance over time<sup>74</sup>, was used to minimize the influence of outliers in all series. Low series replication, often in the earliest portions of a chronology collection, can also inflate the variance of tree-ring records<sup>75</sup>. The one-thirds spline method was chosen when replication in the inner portion of each chronology (the earliest approximately 30–50 years of each record depending on the full chronology length) was less than three trees. When replication was greater than  $n = 3$  trees, we used the average correlation between raw ring-width series (rbar) method. The robust biweight mean chronology (RWI) for each species–site combination was calculated from the ring-width indices following variance stabilization<sup>73</sup>. We defined chronology start year (Extended Data Table 1) as the year in which subsample signal strength passed a threshold of subsample signal strength = 0.8, or where 80% or more of the population signal was captured in the chronology.

For the analysis of correlation between RWI and climate variables, we obtained monthly  $T_{\max}$  and  $T_{\min}$  data for 1901–2019 from CRU v.4.0 (ref. <sup>54</sup>). Correlations between monthly climate and RWI were assessed in R v 4.0 (ref. <sup>76</sup>) using the packages dplR<sup>77</sup> and bootRes<sup>78</sup>. Reported correlations and significance were determined using bootstrapped confidence intervals. Summary figures were created using the package dplR<sup>77</sup> (Fig. 3 and Extended Data Figs. 6 and 7).

Our analysis focused on assessing correlations of RWI to months spanning January to September of the current year (presented in Fig. 3

# Article

and Extended Data Fig. 6). To test for potential lag effects of spring temperatures on growth the following year, we also ran a version of the analysis extending back to include climate of every month of the previous year (Extended Data Fig. 7). Correlations and significance levels for months March–August are given in Supplementary Table 1.

We used a multivariate model to test for joint effects of April and summer  $T_{\max}$  on RWI. We focused on April to represent spring temperatures because it was the month with the greatest overall alignment with the CTWs identified in the dendrometer band analysis and had the highest rate of positive correlations with RWI (Extended Data Table 3). We began by testing univariate correlations of  $T_{\max}$  over three summer windows: June, June–July and May–August. Having determined that, among these, June–July explained the most variation, we then analysed the joint effects of April  $T_{\max}$  and June–July  $T_{\max}$  on RWI for each chronology independently using the base `lm()` function in R. Slopes and  $P$  values for each chronology are given in Supplementary Table 1. Although some models may have benefitted from data transformations, we determined that assumptions of normality and homoscedasticity were sufficiently met for the purposes of this analysis.

## Reporting summary

Further information on research design is available in the Nature Research Reporting Summary linked to this article.

## Data availability

The datasets generated and analysed during the current study are available via GitHub in the `growth_phenology` repository of the ForestGEO Ecosystems & Climate Lab at SCBI ([https://github.com/EcoClimLab/growth\\_phenology](https://github.com/EcoClimLab/growth_phenology)) and archived in Zenodo (<https://doi.org/10.5281/zenodo.6632090>). Master versions of the dendrometer band data are available for SCBI via GitHub in the `Dendrobands` repository of the SCBI ForestGEO plot (<https://github.com/SCBI-ForestGEO/Dendrobands>), which is archived in Zenodo (<https://doi.org/10.5281/zenodo.5551143>), and for Harvard Forest via the Harvard Forest Data Archive (<https://harvardforest1.fas.harvard.edu/exist/apps/datasets/showData.html?id=HF149>). Weather data for SCBI were obtained from the ForestGEO Climate Data Portal v1.0 ([https://github.com/forestgeo/Climate/tree/master/Climate\\_Data/Met\\_Stations/SCBI](https://github.com/forestgeo/Climate/tree/master/Climate_Data/Met_Stations/SCBI)), which is archived in Zenodo (<https://doi.org/10.5281/zenodo.3958215>), and the NCEI weather station located in Front Royal, VA, USA (<https://www.ncdc.noaa.gov/cdo-web/datasets/GHCND/stations/GHCND:USC00443229/detail>). Weather data for Harvard Forest are available through the Harvard Forest Data Archive (<https://harvardforest1.fas.harvard.edu/exist/apps/datasets/showData.html?id=HF001> and <https://harvardforest1.fas.harvard.edu/exist/apps/datasets/showData.html?id=HF000>). Climate data were obtained from CRU v.4.04 via the ForestGEO Climate Data Portal v1.0 ([https://github.com/forestgeo/Climate/tree/master/Climate\\_Data/CRU](https://github.com/forestgeo/Climate/tree/master/Climate_Data/CRU)), which is archived in Zenodo (<https://doi.org/10.5281/zenodo.3958215>). The SPEI was obtained from the ForestGEO Climate Data Portal v1.0 ([https://github.com/forestgeo/Climate/tree/master/Climate\\_Data/SPEI](https://github.com/forestgeo/Climate/tree/master/Climate_Data/SPEI)), which is archived in Zenodo (<https://doi.org/10.5281/zenodo.3958215>). Canopy foliage phenology data were extracted from the MCD12Q2 V6 Land Cover Dynamics product (that is, MODIS Global Vegetation Phenology product) via Google Earth Engine ([https://developers.google.com/earth-engine/datasets/catalog/MODIS\\_006\\_MCD12Q2#description](https://developers.google.com/earth-engine/datasets/catalog/MODIS_006_MCD12Q2#description)). In addition to being archived in the repository for this project, many tree-ring datasets are archived in the International Tree-Ring Data Bank (<https://www.ncpi.noaa.gov/products/paleoclimatology/tree-ring>), the Dendro-Ecological Network (<https://www.uvm.edu/femc/dendro/>) and/or the Harvard Forest Data Archive (<https://harvardforest.fas.harvard.edu/harvard-forest-data-archive>), as detailed in Supplementary Table 1. Original tree cores are archived at the institutions of various members of

the author team (Harvard Forest, SCBI, Indiana University and University of Idaho) and will be made available on reasonable request.

## Code availability

Data were analysed in the open source statistical software R (version 4.0). We used the packages `climwin` v.1.2.3 (<https://cran.r-project.org/web/packages/climwin/index.html>), `dplR` v.1.0.2, `bootRes` v1.2.4, `rstanarm` v.2.21.1 and functions from `Rdendrom` v.0.1.0 (<https://github.com/seanmcm/RDendrom/>). We used `climpact` software v.1.2.8 (see [www.climpact-sci.org](http://www.climpact-sci.org)). Mixed-effect models were run within a hierarchical Bayesian framework and fit using the `rstanarm` version 2.21.3 R interface to the Stan programming language (source code available at [https://github.com/EcoClimLab/growth\\_phenology#steps-to-replicate-the-analysis](https://github.com/EcoClimLab/growth_phenology#steps-to-replicate-the-analysis)). Tree-ring chronologies were developed using the program ARSTAN V49\_1b (<https://www.geog.cam.ac.uk/research/projects/dendrosoftware/>). All custom codes are available through the EcoClimlab GitHub repository ([https://github.com/EcoClimLab/growth\\_phenology](https://github.com/EcoClimLab/growth_phenology)) and archived in Zenodo (<https://doi.org/10.5281/zenodo.6632090>).

51. Bourg, N. A., McShea, W. J., Thompson, J. R., McGarvey, J. C. & Shen, X. Initial census, woody seedling, seed rain, and stand structure data for the SCBI SIGEO Large Forest Dynamics Plot. *Ecology* **94**, 2111–2122 (2013).
52. Anderson-Treixeira, K. J. et al. CTFS-ForestGEO: a worldwide network monitoring forests in an era of global change. *Glob. Chang. Biol.* **21**, 528–549 (2015).
53. Davies, S. J. et al. ForestGEO: understanding forest diversity and dynamics through a global observatory network. *Biol. Conserv.* **253**, 108907 (2021).
54. Harris, I., Osborn, T. J., Jones, P. & Lister, D. Version 4 of the CRU TS monthly high-resolution gridded multivariate climate dataset. *Sci. Data* **7**, 109 (2020).
55. Vicente-Serrano, S. M., Beguería, S. & López-Moreno, J. I. A multiscalar drought index sensitive to global warming: the standardized precipitation evapotranspiration index. *J. Clim.* **23**, 1696–1718 (2010).
56. Herrmann, V. et al. Tree circumference dynamics in four forests characterized using automated dendrometer bands. *PLoS ONE* **11**, e0169020 (2016).
57. Friedl, M., Gray, J. & Sulla-Menashe, D. MCD12Q2 MODIS/Terra+Aqua Land Cover Dynamics Yearly L3 Global 500m SIN Grid V006. LAADS DAAC <https://doi.org/10.5067/MODIS/MCD12Q2.006> (2019).
58. Anderson-Treixeira, K. et al. Forestgeo/Climate: initial release. Zenodo <https://doi.org/10.5281/ZENODO.4041609> (2020).
59. Benestad, R. E., Hanssen-Bauer, I. & Chen, D. *Empirical-Statistical Downscaling* (World Scientific, 2008).
60. Boose, E. & Gould, E. Shaler Meteorological Station at Harvard Forest 1964–2002. *Environmental Data Initiative* <https://doi.org/10.6073/PASTA/213335F5DA17222A738C105B9F60C4> (2021).
61. Boose, E. Fisher Meteorological Station at Harvard Forest since 2001. *Environmental Data Initiative* <https://doi.org/10.6073/PASTA/69E92642B512897032446CFE795CFBB8> (2021).
62. Beguería, S., Vicente-Serrano, S. M., Reig, F. & Latorre, B. Standardized precipitation evapotranspiration index (SPEI) revisited: parameter fitting, evapotranspiration models, tools, datasets and drought monitoring. *Int. J. Climatol.* **34**, 3001–3023 (2014).
63. van de Pol, M. et al. Identifying the best climatic predictors in ecology and evolution. *Methods Ecol. Evol.* **7**, 1246–1257 (2016).
64. Gabry, J. et al. Rstanarm: Bayesian applied regression modeling via Stan. R package version 2.21.1 <https://mc-stan.org/rstanarm> (2020).
65. Stan Development Team. Stan modeling language users guide and reference manual, 2.28. <https://mc-stan.org/users/documentation/> (2019).
66. Stokes, M. A. & Smiley, T. L. *An Introduction to Tree-ring Dating* (Univ. Arizona Press, 1968).
67. Speer, J. H. *Fundamentals of Tree-ring Research* (Univ. Arizona Press, 2010).
68. Alexander, M. R. et al. The potential to strengthen temperature reconstructions in ecoregions with limited tree line using a multispecies approach. *Quat. Res.* **92**, 583–597 (2019).
69. Dye, A. et al. Comparing tree-ring and permanent plot estimates of aboveground net primary production in three eastern U.S. forests. *Ecosphere* **7**, e01454 (2016).
70. Pederson, N. *Climatic Sensitivity and Growth of Southern Temperate Trees in the Eastern United States: Implications for the Carbon Cycle—ProQuest* (Columbia Univ., 2005).
71. Maxwell, J. T. et al. Sampling density and date along with species selection influence spatial representation of tree-ring reconstructions. *Clim. Past* **16**, 1901–1916 (2020).
72. Cook, E. R. & Kairiukstis, L. A. *Methods of Dendrochronology: Applications in the Environmental Sciences* (Springer Netherlands, 1990).
73. Cook, E. R. A Time Series Analysis Approach to Tree Ring Standardization (Univ. Arizona, 1985).
74. Cook, E. R. & Peters, K. Calculating unbiased tree-ring indices for the study of climatic and environmental change. *Holocene* **7**, 361–370 (1997).
75. Jones, P. D., Osborn, T. J. & Briffa, K. R. Estimating sampling errors in large-scale temperature averages. *J. Clim.* **10**, 2548–2568 (1997).
76. R Core Team. *R: A Language and Environment for Statistical Computing*. <http://www.R-project.org/> (R Foundation for Statistical Computing, 2020).
77. Bunn, A. G. A dendrochronology program library in R (dplR). *Dendrochronologia* **26**, 115–124 (2008).
78. Zang, C. & Biondi, F. Dendroclimatic calibration in R: the bootRes package for response and correlation function analysis. *Dendrochronologia* **31**, 68–74 (2013).

**Acknowledgements** We acknowledge all researchers who assisted with data collection in the field and laboratory, particularly T. Fung Au, J. Bregy, J. Dickens, K. Heeter, A. Hennage, D. King, J. McGee, B. Lockwood, J. McGarvey, V. Meakem, J. Oliver, J. Shue, K. Schmidt-Simard, B. Strange, A. Terrell, B. Taylor, M. Thornton, S. Robeson, M. Wenzel and L. Wylie; and D. A. Orwig, R. Zweifel and members of the ForestGEO Ecosystems & Climate Lab at SCBI for helpful feedback. Analyses and SCBI data collection were funded by the Smithsonian Institution (ForestGEO—Smithsonian Tropical Research Institute, Smithsonian’s National Zoo & Conservation Biology Institute, and Scholarly Studies, Competitive Grants Program for Science and Grand Challenges Award Program grants to K.J.A.-T.). Collection of tree-ring samples was funded by the USDA Agriculture and Food Research Initiative grant 2017-67013-26191 (to J.T.M.), National Science Foundation grants nos. 1805276 (to G.L.H.) and 1805617 (to J.T.M.), and from the Indiana University Vice Provost for Research Faculty Research Program (to J.T.M.). L.D. received funding from the Natural Sciences and Engineering Research Council of Canada (DG RGPIN-2019-04353) and New Brunswick Innovation Foundation (RIF 2019-029). S.M.M. was partially funded by National Science Foundation RAPID-2030862.

**Author contributions** C.D. and K.J.A.-T. conceived the ideas and designed the study. C.D., L.D., E.B.G.-A., R.H., G.L.H., J.T.M., I.R.M., W.J.M., N.P., A.J.T. and K.J.A.-T. collected or oversaw collection of data. C.D., A.Y.K., V.H., J.T.M., I.R.M. and S.M.M. analysed the data or provided analytical tools. C.D. and K.J.A.-T. led the writing of the manuscript. All authors contributed critically to the drafts and gave final approval for publication.

**Competing interests** The authors declare no competing interests.

**Additional information**

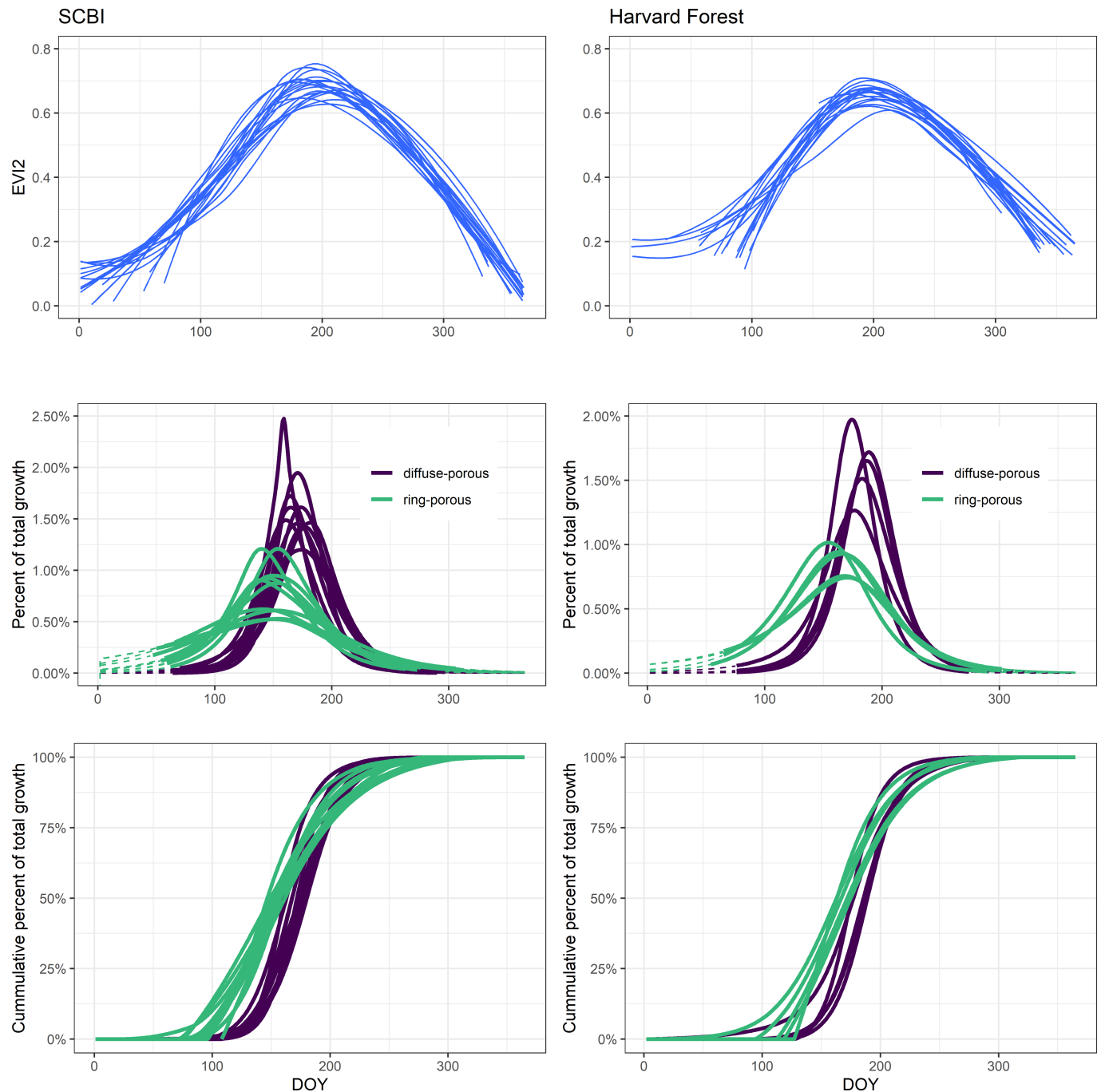
**Supplementary information** The online version contains supplementary material available at <https://doi.org/10.1038/s41586-022-05092-3>.

**Correspondence and requests for materials** should be addressed to Kristina J. Anderson-Texeira.

**Peer review information** *Nature* thanks Cyrille Rathgeber, Roman Zweifel and the other, anonymous, reviewer(s) for their contribution to the peer review of this work. Peer reviewer reports are available.

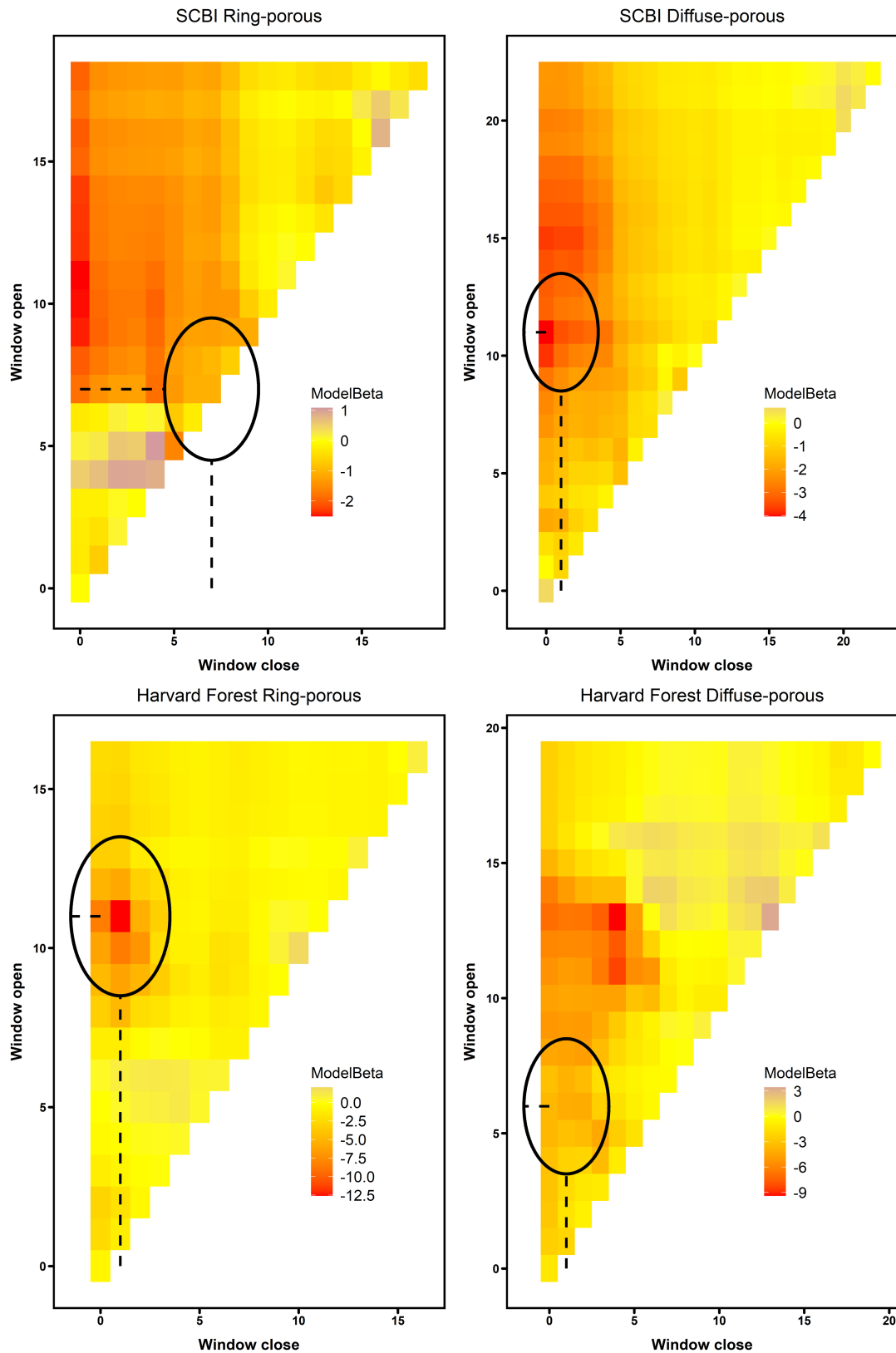
**Reprints and permissions information** is available at <http://www.nature.com/reprints>.

# Article



**Extended Data Fig. 1 | Seasonal patterns of forest canopy greenness (top row) and stem growth of ring- and diffuse-porous trees, represented as both relative and cumulative fractions of total annual growth (middle and bottom rows, respectively), at the Smithsonian Conservation Biology Institute (SCBI) and Harvard Forest.** In the top row, canopy greenness is characterized using the two band Enhanced Vegetation Index (EVI2), with each

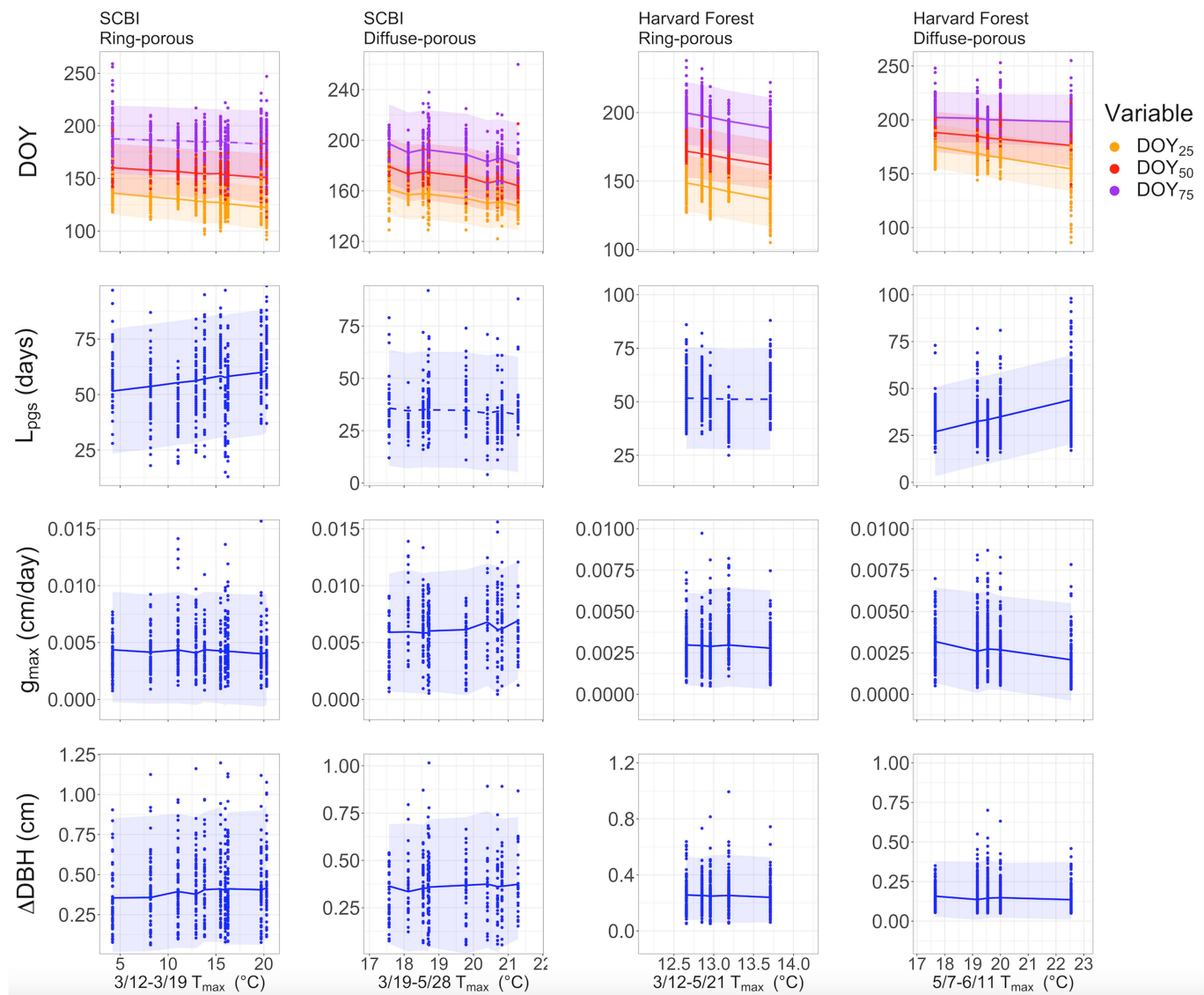
line representing a year between 2000 and 2018. For stem growth, each line represents the average growth over one year, as modeled based on a five-parameter logistic growth model to dendrometer band data. Dashed lines represent modeled DBH change which fell outside of the median DOY where predicted starting and ending DBHs were reached. Solid lines represent DBH change attributable to stem growth.



**Extended Data Fig. 2 | Landscapes of relationships between the day of year on which 25% of annual growth is achieved ( $DOY_{25}$ ) and temperature in prior weeks for ring- and diffuse-porous trees at the Smithsonian Conservation Biology Institute (SCBI) and Harvard Forest.** Shown are matrices of  $\beta$  coefficients from first-order linear regressions between mean maximum temperature ( $T_{max}$ ) and  $DOY_{25}$ . Window Open and Window Close indicate number of weeks prior to  $DOY_{25}$  (listed in Extended Data Table 2). Yellow

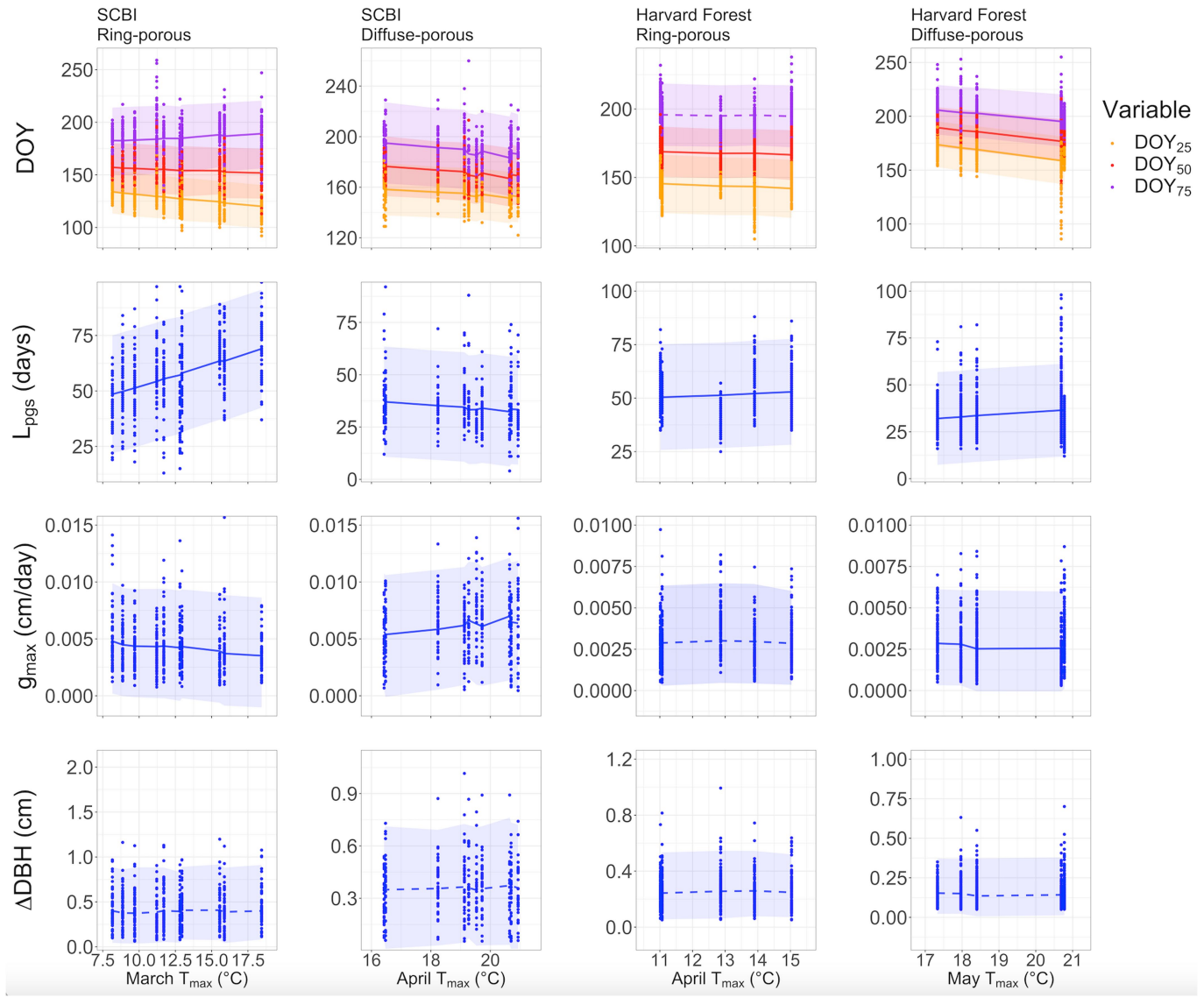
shading indicates neutral relationships, while orange or red shading indicates that  $DOY_{25}$  advances with increased  $T_{max}$  over the given time window (negative  $\beta$ ). Black circles indicate the critical temperature window selected based on minimization of  $\Delta AIC_c$ , the difference in Akaike Information Criterion corrected for small sample size relative to a null model. Critical temperature windows are listed in Extended Data Table 2.

# Article



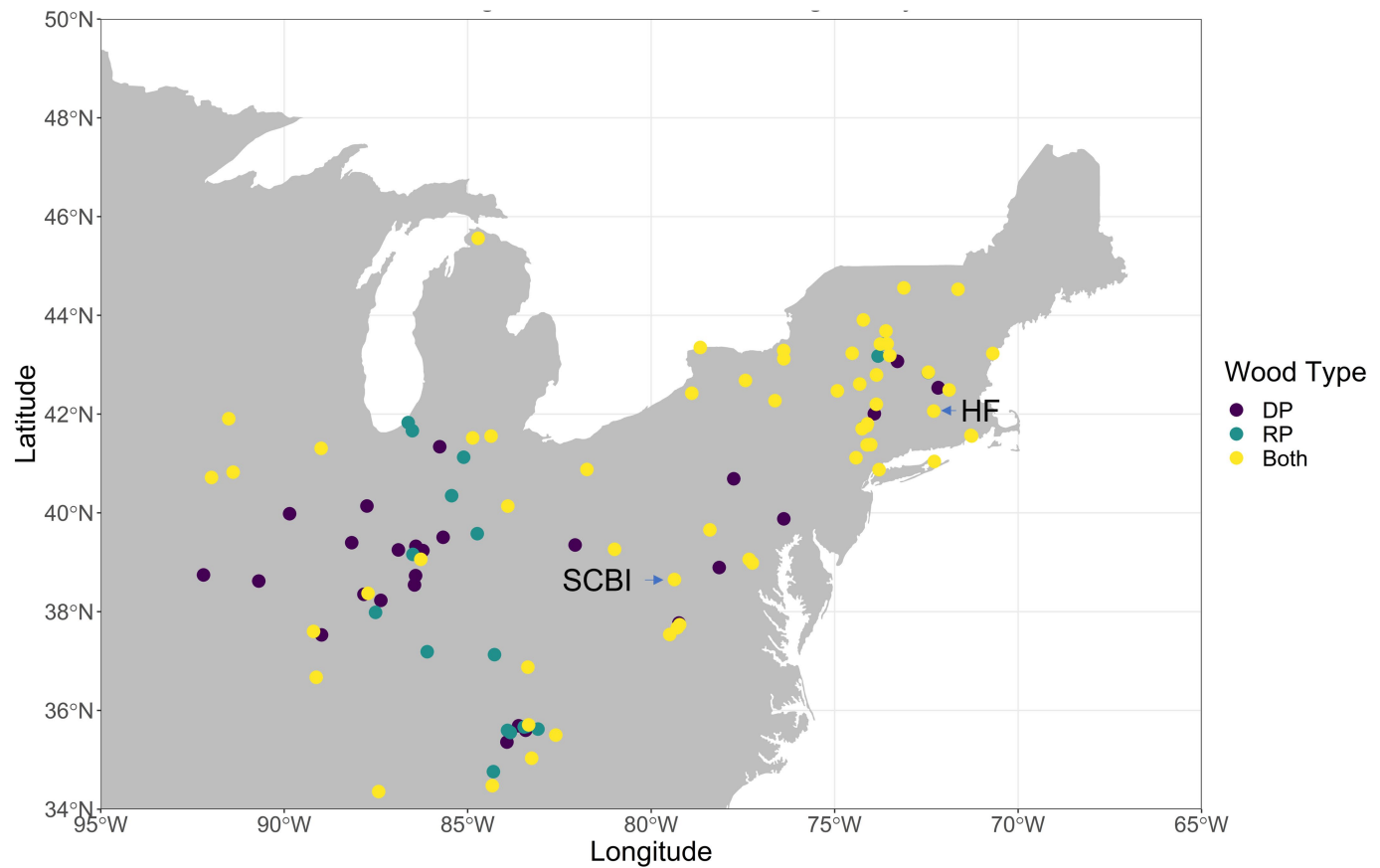
**Extended Data Fig. 3 | Response of stem growth timing and rates to mean maximum temperatures ( $T_{max}$ ) during the spring critical temperature window (CTW) for ring- and diffuse-porous species at the Smithsonian Conservation Biology Institute (SCBI) and Harvard Forest.** CTW was defined as the period over which  $T_{max}$  was most strongly correlated with the day of year on which 25% of annual growth was achieved (DOY<sub>25</sub>; Extended Data Table 2, Extended Data Fig. 2). Shown are relationships between mean  $T_{max}$  over the CTW and days of the year on which 25%, 50%, and 75% total stem growth were achieved (DOY<sub>25</sub>, DOY<sub>50</sub>, DOY<sub>75</sub>, respectively; first row); the length of the peak

growing season ( $L_{pgs}$ ; second row); maximum growth rate ( $g_{max}$ ; third row); and total seasonal radial stem growth ( $\Delta DBH$ ; fourth row). Posterior predictions of each variable that did not include zero are represented with solid lines, while those that do include zero use dotted lines. The 95% credible intervals are represented by bands centered on the posterior mean for each year. For both species groups at both sites, DOY<sub>25</sub>, DOY<sub>50</sub>, and DOY<sub>75</sub> all declined significantly with mean  $T_{max}$  during their respective CTW. Dots represent growth parameter values for individual tree-year combinations, which were derived by fitting a five-parameter logistic growth model to dendrometer band data.

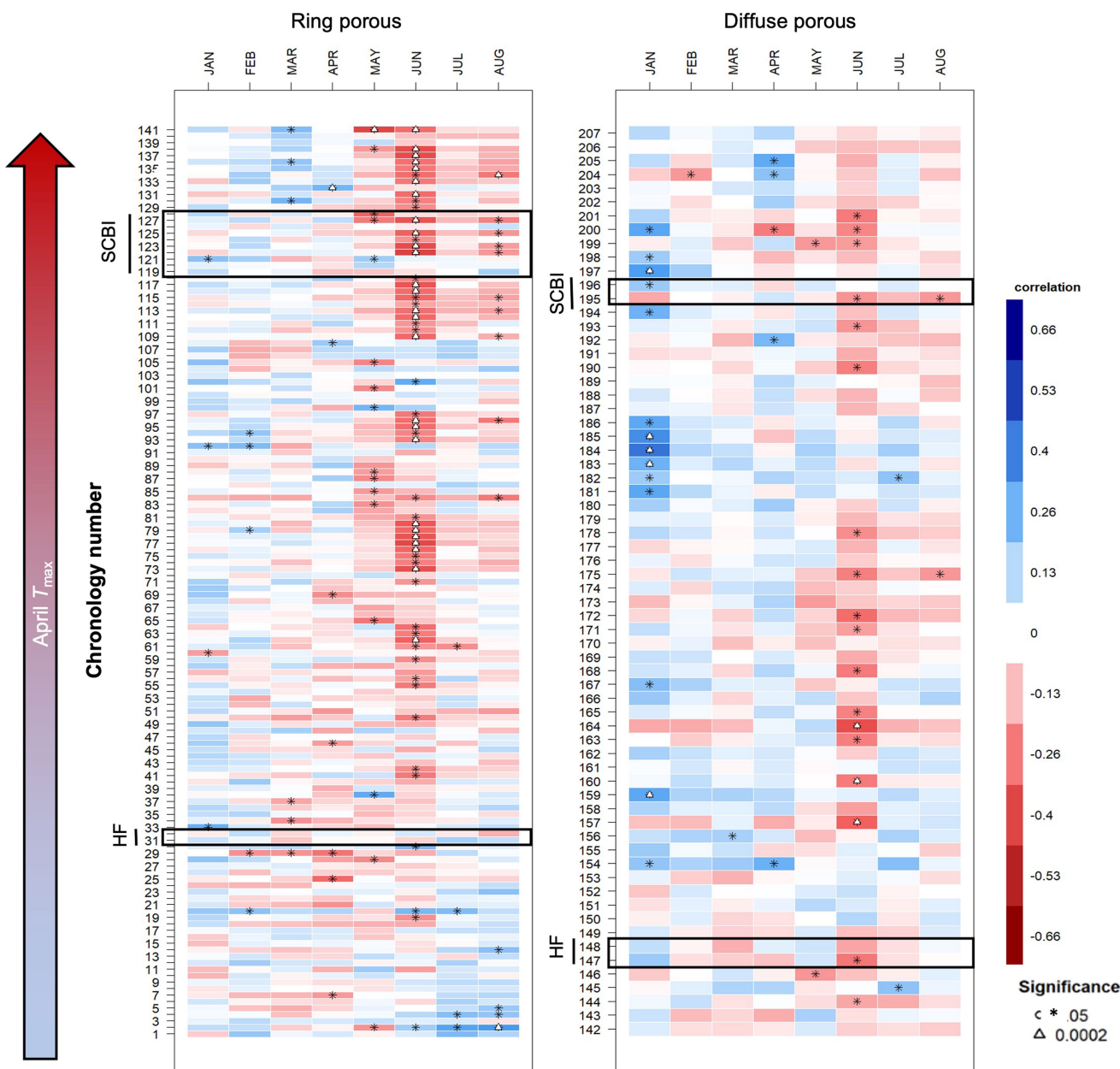


**Extended Data Fig. 4 | Response of stem growth timing and rates to mean maximum temperatures ( $T_{max}$ ) for the month most closely corresponding to the spring critical temperature window (CTW) for ring- and diffuse-porous species at the Smithsonian Conservation Biology Institute (SCBI) and Harvard Forest.** CTW was defined as the period over which  $T_{max}$  was most strongly correlated with the day of year on which 25% of annual growth was achieved ( $DOY_{25}$ ; Extended Data Table 2, Extended Data Fig. 2), and the most closely corresponding month was determined as that with the greatest number of days within the CTW. Shown are relationships between monthly  $T_{max}$  and days of the year on which 25%, 50%, and 75% total stem growth were achieved

( $DOY_{25}$ ,  $DOY_{50}$ ,  $DOY_{75}$ , respectively; first row); the length of the peak growing season ( $L_{pgs}$ ; second row); maximum growth rate ( $g_{max}$ ; third row); and total seasonal radial stem growth ( $\Delta DBH$ ; fourth row). Posterior predictions of each variable that did not include zero are represented with solid lines, while those that do include zero use dotted lines. The 95% credible intervals are represented by bands centered on the posterior mean for each year. For both species groups at both sites,  $DOY_{25}$ ,  $DOY_{50}$ , and  $DOY_{75}$  declined significantly with April  $T_{max}$  with the exception of  $DOY_{25}$  for ring-porous species at SCBI. Dots represent growth parameter values for individual tree-year combinations, which were derived by fitting a five-parameter logistic growth model to dendrometer band data.

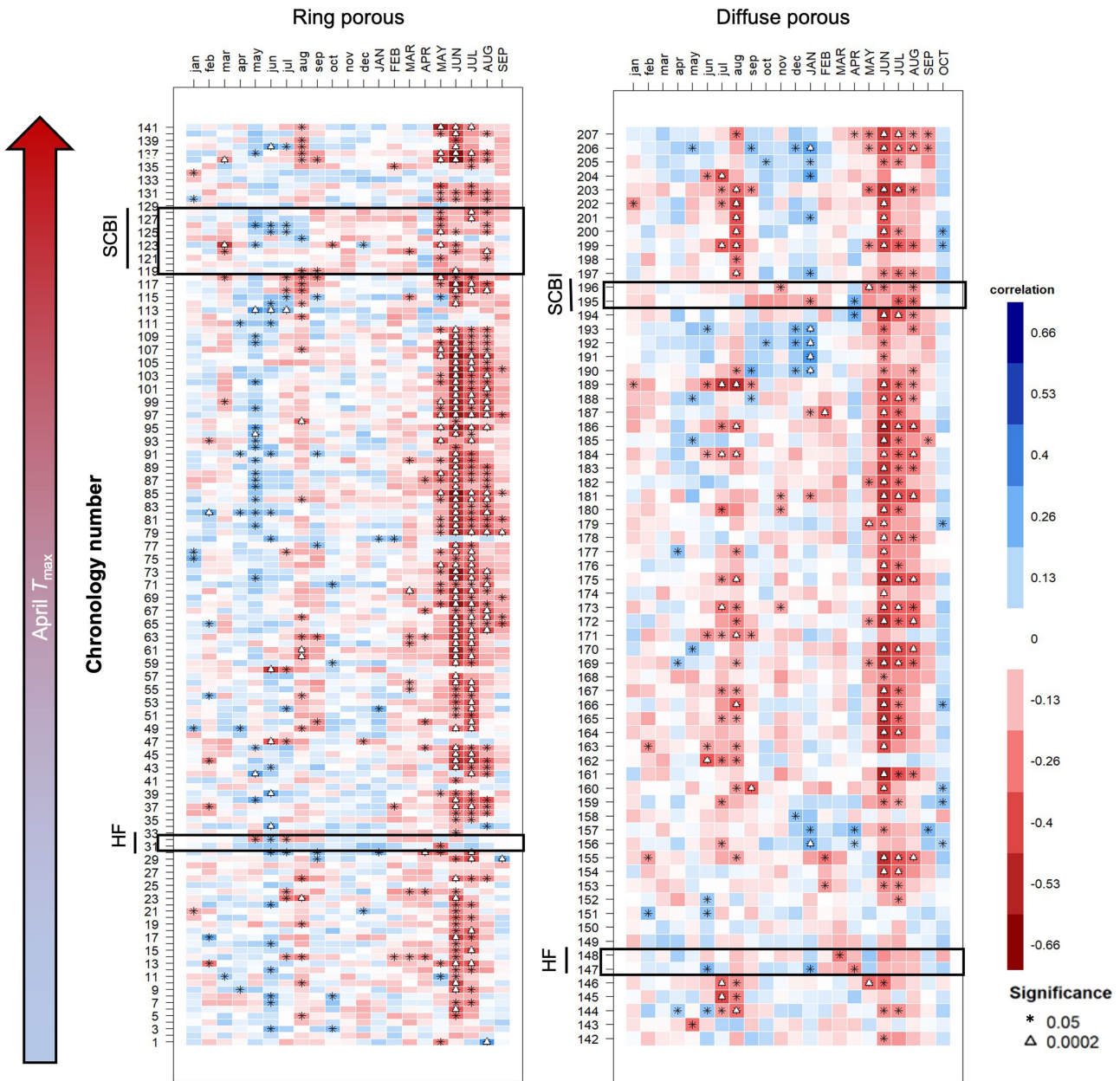


**Extended Data Fig. 5 | Map of sampling locations of tree-ring chronologies analyzed in this study.** Sites are colored by the xylem porosity type of species sampled: ring porous (RP), diffuse porous (DP), or both. Sampling details are provided in Supplementary Table 1. Base map source is ggplot2.



**Extended Data Fig. 6 | Sensitivity of annual growth, as derived from tree-rings, to monthly mean minimum temperatures ( $T_{min}$ ), for 207 chronologies from 108 sites across eastern North America (Extended Data Fig. 5).**  
Colors indicate the bootstrapped correlation between monthly  $T_{min}$  and a dimensionless ring width index ( $RWI$ ) derived from the multiple trees that form each chronology and emphasizing interannual variability associated with

climate. Chronologies are grouped by xylem porosity and ordered by mean April  $T_{min}$ . Plots are annotated to highlight records from our two focal sites, the Smithsonian Conservation Biology Institute (SCBI) and Harvard Forest (HF) (Extended Data Table 1). Species analyzed and numbers of significant correlations to  $T_{min}$  are summarized in Extended Data Table 3, and chronology details are given in Supplementary Table 1.



**Extended Data Fig. 7 | Sensitivity of annual growth, as derived from tree-rings, to monthly mean maximum temperatures ( $T_{max}$ ) of the current and past year, for 207 chronologies from 108 sites across eastern North America (Extended Data Fig. 5).** Colors indicate the bootstrapped correlation between monthly  $T_{max}$  and a dimensionless ring width index ( $RWI$ ) derived from the multiple trees that form each chronology and emphasizing interannual variability associated with climate. Chronologies are grouped by xylem

porosity and ordered by mean April  $T_{max}$ . Plots are annotated to highlight records from our two focal sites, the Smithsonian Conservation Biology Institute (SCBI) and Harvard Forest (HF) (Extended Data Table 1). Figure presents the same results as Fig. 3 but extends back to include the previous year. Species analyzed and numbers of significant correlations to  $T_{max}$  are summarized in Extended Data Table 3, and chronology details are given in Supplementary Table 1.

**Extended Data Table 1 | Dominant broadleaf deciduous species at the Smithsonian Conservation Biology Institute (SCBI) and Harvard Forest, along with sample sizes included in our final analysis**

	species	dendrometer bands		tree cores	
		n trees	n tree-years	n cores	date range
<b>SCBI</b>					
ring-porous	<i>Carya cordiformis</i>	0	0	18	1917-2009
	<i>Carya glabra</i>	0	0	39	1901-2009
	<i>Carya ovalis</i>	0	0	24	1896-2009
	<i>Carya tomentosa</i>	0	0	17	1926-2009
	<i>Fraxinus nigra</i>	0	0	16	1901-2016
	<i>Fraxinus americana</i>	0	0	69	1910-2009
	<i>Quercus alba</i>	34	272	66	1904-2009
	<i>Quercus montana</i>	0	0	67	1893-2009
	<i>Quercus rubra</i>	33	265	71	1870-2009
	<i>Quercus velutina</i>	0	0	83	1902-2009
diffuse-porous	<i>Fagus grandifolia</i>	13	75	81	1932-2009
	<i>Liriodendron tulipifera</i>	39	292	109	1920-2009
<b>Harvard Forest</b>					
ring-porous	<i>Fraxinus americana</i>	8	28	34	1901-2008
	<i>Quercus rubra</i>	119	529	179	1901-2014
	<i>Quercus velutina</i>	11	53	0	
diffuse-porous	<i>Fagus grandifolia</i>	8	35	0	
	<i>Betula lenta</i>	8	37	0	
	<i>Betula populifolia</i>	5	16	0	
	<i>Betula papyrifera</i>	3	10	0	
	<i>Betula alleghaniensis</i>	19	72	44	1952-2013
	<i>Prunus serotina</i>	8	29	0	
	<i>Acer rubrum</i>	128	477	59	1930-2014
	<i>Acer pensylvanicum</i>	4	13	0	

# Article

**Extended Data Table 2 | Summary of parameters describing the seasonality and temperature sensitivity of broadleaf deciduous tree woody growth and canopy phenology at the Smithsonian Conservation Biology Institute (SCBI) and Harvard Forest**

	SCBI		Harvard Forest	
	ring-porous	diffuse-porous	ring-porous	diffuse-porous
critical $T_{max}$ window	3/5-3/19	3/19-5/28	3/12-5/21	5/7-6/11
<b>Stem Growth</b>				
$DOY_{25}$	128 (May 8)	155 (June 5)	144 (May 24)	166 (June 16)
$DOY_{50}$	154 (June 4)	172 (June 22)	168 (June 17)	183 (July 3)
$DOY_{75}$	185 (July 4)	190 (July 9)	195 (July 14)	201 (July 20)
$g_{max}$ (cm/day)	0.0043	0.0061	0.003	0.003
$L_{pgs}$	57.3	34.8	51.3	34.4
$\Delta DBH$ (cm/yr)	0.41	0.36	0.26	0.16
<b>Canopy Foliage (ecosystem level)</b>				
Greenup	101 (April 11)		115 (April 25)	
Mid-greenup	121 (May 1)		137 (May 17)	
Peak	173 (June 22)		182 (July 1)	
Senescence	215 (Aug. 3)		218 (Aug. 6)	
<b>Temperature sensitivity (days/<math>^{\circ}\text{C}</math>)</b>				
Stem growth:				
$DOY_{25}$	$-1.7 \pm 0.13$	$-2.8 \pm 0.39$	$-12.3 \pm 0.91$	$-4.2 \pm 0.22$
$DOY_{50}$	$-1 \pm 0.13$	$-2.9 \pm 0.4$	$-10.3 \pm 0.74$	$-2.5 \pm 0.17$
$DOY_{75}$	$0.08 \pm 0.19$	$-2.9 \pm 0.6$	$-11.1 \pm 0.96$	$-0.9 \pm 0.23$
$\Delta DBH$ (cm/ $^{\circ}\text{C}$ )	$.003 \pm .001$	$.008 \pm .004$	$-.027 \pm .004$	$-.003 \pm .001$
Canopy foliage:				
Greenup	$3.45 \pm 1.29$		$2.4 \pm 1.51$	
Mid-greenup	$3.39 \pm 0.86$		$3.16 \pm 0.84$	
Peak	$4.21 \pm 1.70$		$1.47 \pm 1.02$	
Senescence	$3.85 \pm 2.13$		$0.17 \pm 1.53$	

Temperature sensitivity refers to the sensitivity of a parameter to the mean maximum temperature ( $T_{max}$ ) during the critical temperature window (CTW, Fig. 1). Because leaf phenology measurements were derived from satellite imagery and included both ring- and diffuse-porous trees, the selection of a critical window was less straightforward. We used the CTW of the porosity group containing the dominant canopy species at each site: *Liriodendron tulipifera* (diffuse porous) at SCBI and *Quercus rubra* (ring porous) at Harvard Forest.

**Extended Data Table 3 | Summary of tree-ring chronologies analyzed and number of significant (at significance level = 0.05) positive or negative correlations of ring width index to monthly  $T_{max}$  in univariate and multivariate analyses**

		n. significant bootstrapped correlations of RWI to monthly mean max. T															
species	n	univariate analysis												multivariate analysis			
		March		April		May		June		July		Aug		April		June-July	
<b>Ring-porous</b>																	
<i>Carya cordiformis</i>	1	0	0	0	0	0	1	0	1	0	0	0	0	0	0	0	1
<i>Carya glabra</i>	7	0	0	0	0	0	3	0	5	0	5	0	0	0	0	0	5
<i>Carya ovalis</i>	1	0	0	1	0	0	1	0	0	0	0	0	0	1	0	0	0
<i>Carya ovata</i>	21	0	2	0	0	0	5	0	20	0	17	0	12	2	0	0	20
<i>Carya tomentosa</i>	2	0	1	0	0	0	1	0	2	0	0	0	2	0	0	0	1
<i>Fraxinus americana</i>	5	0	1	0	0	0	4	0	3	0	2	1	0	0	0	0	3
<i>Fraxinus nigra</i>	2	0	0	0	0	0	0	0	1	0	1	0	1	0	0	0	1
<i>Quercus alba</i>	35	0	2	0	4	0	18	0	31	0	29	0	23	0	2	0	33
<i>Quercus bicolor</i>	1	0	0	0	0	0	0	0	0	0	1	0	1	0	0	0	0
<i>Quercus macrocarpa</i>	1	0	0	0	0	0	0	0	1	0	1	0	1	0	0	0	1
<i>Quercus montana</i>	17	0	1	0	2	1	4	0	10	0	9	0	3	1	2	0	11
<i>Quercus pagoda</i>	1	0	0	0	0	0	1	0	1	0	1	0	1	0	0	0	1
<i>Quercus rubra</i>	37	0	3	0	2	1	4	0	25	0	18	1	5	1	1	0	22
<i>Quercus</i> sp (white oak group)	1	0	0	0	0	0	0	0	1	0	0	0	0	0	0	0	1
<i>Quercus stellata</i>	2	0	0	0	0	0	1	0	1	0	1	0	0	0	0	0	1
<i>Quercus velutina</i>	7	0	0	0	0	0	2	0	5	0	6	0	3	0	0	0	7
TOTAL	141	0	10	1	8	2	45	0	107	0	91	2	53	4	5	0	108
<b>Diffuse-porous</b>																	
<i>Acer rubrum</i>	4	0	0	0	1	0	0	0	1	0	1	0	0	0	1	0	3
<i>Acer saccharum</i>	16	0	0	1	0	0	2	0	14	0	12	0	6	3	0	0	14
<i>Betula alleghaniensis</i>	2	0	0	0	0	0	0	0	2	0	0	0	0	0	0	0	1
<i>Betula lenta</i>	3	0	0	0	0	0	1	0	1	0	1	0	0	0	0	0	2
<i>Fagus grandifolia</i>	6	0	0	1	0	0	0	0	4	0	5	0	1	1	0	0	5
<i>Liriodendron tulipifera</i>	32	0	0	2	1	0	7	0	30	0	17	0	16	1	0	0	27
<i>Magnolia acuminata</i>	1	0	0	0	0	0	0	0	0	0	0	0	0	0	0	0	0
<i>Nyssa sylvatica</i>	1	0	0	0	0	0	0	0	0	0	0	0	0	0	0	0	0
<i>Populus grandidentata</i>	1	0	0	0	0	0	0	0	0	0	0	0	0	0	0	0	0
TOTAL	66	0	0	4	2	0	10	0	52	0	36	0	23	5	1	0	52
TOTAL	207	0	10	5	10	2	55	0	159	0	127	2	76	9	6	0	160

## Reporting Summary

Nature Portfolio wishes to improve the reproducibility of the work that we publish. This form provides structure for consistency and transparency in reporting. For further information on Nature Portfolio policies, see our [Editorial Policies](#) and the [Editorial Policy Checklist](#).

### Statistics

For all statistical analyses, confirm that the following items are present in the figure legend, table legend, main text, or Methods section.

n/a Confirmed

- The exact sample size ( $n$ ) for each experimental group/condition, given as a discrete number and unit of measurement
- A statement on whether measurements were taken from distinct samples or whether the same sample was measured repeatedly
- The statistical test(s) used AND whether they are one- or two-sided  
*Only common tests should be described solely by name; describe more complex techniques in the Methods section.*
- A description of all covariates tested
- A description of any assumptions or corrections, such as tests of normality and adjustment for multiple comparisons
- A full description of the statistical parameters including central tendency (e.g. means) or other basic estimates (e.g. regression coefficient) AND variation (e.g. standard deviation) or associated estimates of uncertainty (e.g. confidence intervals)
- For null hypothesis testing, the test statistic (e.g.  $F$ ,  $t$ ,  $r$ ) with confidence intervals, effect sizes, degrees of freedom and  $P$  value noted  
*Give P values as exact values whenever suitable.*
- For Bayesian analysis, information on the choice of priors and Markov chain Monte Carlo settings
- For hierarchical and complex designs, identification of the appropriate level for tests and full reporting of outcomes
- Estimates of effect sizes (e.g. Cohen's  $d$ , Pearson's  $r$ ), indicating how they were calculated

*Our web collection on [statistics for biologists](#) contains articles on many of the points above.*

### Software and code

Policy information about [availability of computer code](#)

Data collection	No software was used for data collection.
Data analysis	Data were analysed in the open source statistical software R (version 4.0). We used packages climwin v.1.2.3 ( <a href="https://cran.r-project.org/web/packages/climwin/index.html">https://cran.r-project.org/web/packages/climwin/index.html</a> ), dplR v.1.0.2, and bootRes v1.2.4, rstanarm v.2.21.1, and functions from Rdendrom v.0.1.0 ( <a href="https://github.com/seanmcm/RDendrom/">https://github.com/seanmcm/RDendrom/</a> ). We used climpact software v.1.2.8 (see <a href="http://www.climpact-sci.org">www.climpact-sci.org</a> ). Mixed effects models were run with mixed-effect model was run within a hierarchical Bayesian framework and fit using the rstanarm version 2.21.3 R interface to the Stan programming language (source code available at <a href="https://github.com/EcoClimLab/growth_phenology#steps-to-replicate-the-analysis">https://github.com/EcoClimLab/growth_phenology#steps-to-replicate-the-analysis</a> ). Tree-ring chronologies were developed using the program ARSTAN V49_1b ( <a href="https://www.geog.cam.ac.uk/research/projects/dendrosoftware/">https://www.geog.cam.ac.uk/research/projects/dendrosoftware/</a> ). All custom code is available through the EcoClimlab GitHub repository ( <a href="https://github.com/EcoClimLab/growth_phenology">https://github.com/EcoClimLab/growth_phenology</a> ) and archived in Zenodo (DOI: 10.5281/zenodo.6632090).

For manuscripts utilizing custom algorithms or software that are central to the research but not yet described in published literature, software must be made available to editors and reviewers. We strongly encourage code deposition in a community repository (e.g. GitHub). See the Nature Portfolio [guidelines for submitting code & software](#) for further information.

## Data

Policy information about [availability of data](#)

All manuscripts must include a [data availability statement](#). This statement should provide the following information, where applicable:

- Accession codes, unique identifiers, or web links for publicly available datasets
- A description of any restrictions on data availability
- For clinical datasets or third party data, please ensure that the statement adheres to our [policy](#)

The datasets generated and analysed during the current study are available via GitHub in the growth\_phenology repository of the ForestGEO Ecosystems & Climate Lab @ SCBI, ([https://github.com/EcoClimLab/growth\\_phenology](https://github.com/EcoClimLab/growth_phenology)) and archived in Zenodo (DOI: 10.5281/zenodo.6632090). Master versions of the dendrometer band data are available for SCBI via GitHub in the Dendrobands repository of the Smithsonian Conservation Biology Institute ForestGEO plot (<https://github.com/SCBI-ForestGEO/Dendrobands>), which is archived in Zenodo (DOI 10.5281/zenodo.5551143), and for Harvard Forest via the Harvard Forest Data Archive (<https://harvardforest1.fas.harvard.edu/exist/apps/datasets/showData.html?id=HF149>). Weather data for SCBI were obtained from the ForestGEO Climate Data Portal v1.0 ([https://github.com/forestgeo/Climate/tree/master/Climate\\_Data/Met\\_Stations/SCBI](https://github.com/forestgeo/Climate/tree/master/Climate_Data/Met_Stations/SCBI)), which is archived in Zenodo (DOI: 10.5281/zenodo.3958215), and the National Center for Environmental Information (NCEI) weather station located in Front Royal, Virginia (<https://www.ncdc.noaa.gov/cdo-web/datasets/GHCND/stations/GHCND:USC00443229/detail>). Weather data for Harvard Forest are available through the Harvard Forest Data Archive (<https://harvardforest1.fas.harvard.edu/exist/apps/datasets/showData.html?id=HF001> AND <https://harvardforest1.fas.harvard.edu/exist/apps/datasets/showData.html?id=HF000>). Climate data were obtained from CRU v.4.04 via the ForestGEO Climate Data Portal v1.0 ([https://github.com/forestgeo/Climate/tree/master/Climate\\_Data/CRU](https://github.com/forestgeo/Climate/tree/master/Climate_Data/CRU)), which is archived in Zenodo (DOI: 10.5281/zenodo.3958215). The Standardised Precipitation-Evapotranspiration Index was obtained from the ForestGEO Climate Data Portal v1.0 ([https://github.com/forestgeo/Climate/tree/master/Climate\\_Data/SPEI](https://github.com/forestgeo/Climate/tree/master/Climate_Data/SPEI)), which is archived in Zenodo (DOI: 10.5281/zenodo.3958215). Canopy foliage phenology data were extracted from the MCD12Q2 V6 Land Cover Dynamics product (a.k.a. MODIS Global Vegetation Phenology product) via Google Earth Engine ([https://developers.google.com/earth-engine/datasets/catalog/MODIS\\_006\\_MCD12Q2#description](https://developers.google.com/earth-engine/datasets/catalog/MODIS_006_MCD12Q2#description)). In addition to being archived in this project's repository, many tree-ring data sets are archived in the International Tree-Ring Data Bank (ITRDB;<https://www.nciee.noaa.gov/products/paleoclimatology/tree-ring>), the DendroEcological Network (DEN; <https://www.uvm.edu/femc/dendro/>), and/or the Harvard Forest Data Archive (<https://harvardforest.fas.harvard.edu/harvard-forest-data-archive>), as detailed in SI Table 1. Original tree cores are archived at the institutions of various members of the author team (Harvard Forest, Smithsonian Conservation Biology Institute, Indiana University, and University of Idaho) and will be made available upon reasonable request.

## Field-specific reporting

Please select the one below that is the best fit for your research. If you are not sure, read the appropriate sections before making your selection.

Life sciences       Behavioural & social sciences       Ecological, evolutionary & environmental sciences

For a reference copy of the document with all sections, see [nature.com/documents/nr-reporting-summary-flat.pdf](https://nature.com/documents/nr-reporting-summary-flat.pdf)

## Ecological, evolutionary & environmental sciences study design

All studies must disclose on these points even when the disclosure is negative.

### Study description

Using dendrometer band measurements from 440 trees across two forests, we show that warmer spring temperatures shifted the woody growth of deciduous trees earlier but had no consistent effect on peak growing season length, maximum daily growth rates, or annual growth. The latter finding was confirmed on the centennial scale by 207 tree-ring chronologies from 108 forests across eastern North America, where annual growth was far more sensitive to temperatures during the peak growing season than in the spring.

### Research sample

Overall, our research sampling was designed to represent dominant temperate broadleaf deciduous trees of North America. The focus was on large individuals with their crowns in the canopy, but smaller trees were included when data were available.

Dendrometer band measurements were made at two sites: Smithsonian Conservation Biology Institute (SCBI; VA) and Harvard Forest (MA), selected because they were the only two sites of which we were aware with multiple years of currently available intra-annual dendrometer band measurements. Both sites are dominated by common species of the temperate deciduous biome of eastern North America. Dendrometer band measurements were made on dominant broadleaf tree species at each site.

Tree core chronologies were created using cores from 108 sites across eastern North America: our two focal sites and an additional 106 sites for which tree-ring chronologies had already been developed. This data set included the largest previously published collection for the biome (D'Orangeville et al. 2018), along with other published and unpublished records developed over the years by the coauthor team. The sample was designed to maximize coverage of temperate broadleaf deciduous forests in eastern N. America, and we did not exclude any available chronologies.

### Sampling strategy

Dendrometer bands:

At SCBI, dendrometer bands were installed on individuals of the two most dominant (in terms of contributions to woody productivity) ring-porous species (*Quercus alba* and *Quercus rubra*) and the two most dominant diffuse-porous species (*Liriodendron tulipifera* and *Fagus grandifolia*). Sampling was weighted towards large individuals. Banded trees were randomly located throughout the 25.6 ha ForestGEO plot, with some additional individuals within two 15 m radius plots in which all trees were banded. Details are available in Extended Data Table 1 and the SCBI-ForestGEO dendrobands repository (<https://github.com/SCBI-ForestGEO/Dendrobands>).

At Harvard Forest, dendrometer bands were placed on trees in 36 circular, 10-m radius plots located randomly along eight 500-m

transects that extended from the EMS eddy-flux tower (detailed in D'Orangeville et al., 2021; <https://doi.org/10.1093/treephys/tpab101>). We analyzed data for eight diffuse- and three ring-porous species (see Extended Data Table 1).

#### Tree cores:

At SCBI, we sampled the 12 species contributing most to woody productivity, sampling live and dead individuals randomly located throughout the plot (detailed in Helcoski et al. 2019; <https://doi.org/10.1111/nph.15906>). At Harvard Forest, all trees were cored within size-stratified circular plots (detailed in Dye et al. 2016; <https://doi.org/10.1002/ecs2.1454>).

The tree-ring records from our focal sites were complemented with a much larger collection of tree-ring chronologies spanning 106 deciduous and mixed forest sites in eastern North America, including both previously published (see Pederson 2005 PhD dissertation; D'Orangeville et al. 2018: <https://doi.org/10.1111/gcb.14096>; Maxwell et al. 2020: <https://doi.org/10.5194/cp-16-1901-2020>) and new chronologies. All of these samples were originally collected for other research projects, many for the estimation of the response of trees and species to climatic variation, and opportunistically included here. For the majority of sampled populations (i.e., site-species combinations), sampling focused on canopy trees (typically >20 trees per population), while ~15% of the total 207 chronologies came from plot-level collections where trees above a certain diameter (typically 10 cm DBH) were censused and cored.

### Data collection

#### Dendrometer bands:

Metal dendrometer bands were installed on a total of 941 trees within the SCBI and Harvard ForestGEO plots. They were placed at ~1.4 m above the base of the tree. Band windows were measured with a digital caliper approximately every 1-2 weeks within the growing season from 2011-2020 at SCBI and 1998-2003 at Harvard Forest. Measurements were made by many collaborators, including research scientists, field technicians, students, and interns. Data were recorded on paper data sheets for subsequent transfer to digital files or directly into digital files using iPads. The number of bands measured at each site fluctuated slightly as trees were added or dropped from the census (e.g., because of tree mortality). Across years, the number of bands sampled averaged 129 (range: 91-138) at SCBI and 717 (range: 700-755) at Harvard Forest. In total, after data cleaning, our analysis included 2210 tree-years (Extended Data Table 1).

Measurements were timed to begin before the beginning of spring growth and to continue through the cessation of growth in the fall. At SCBI, the median start date was April 14, which was adjusted forward when early leaf-out of understory vegetation was observed, with the earliest start date being March 30 (in 2020). Measurements were continued through to fall leaf senescence, with the median end date being October 17 and the latest end date November 26 (2012). At Harvard Forest, all measurements from 1998 were dropped because of a late start date (May 26). Among the remaining years, the median start date was April 21 and median end date of October 27. 1999 was an anomalous year where initial measurements were taken on January 5, but not taken again until April 15. The latest end date was November 11, 2002.

#### Leaf phenology:

Canopy foliage phenology data for the years 2001-2018 were extracted for SCBI and Harvard Forest from the MCD12Q2 V6 Land Cover Dynamics product (a.k.a. MODIS Global Vegetation Phenology product; Friedl et al. 2019, doi: DOI: 10.5067/MODIS/MCD12Q2.006) via Google Earth Engine. For each year at each site, we extracted data from the pixel containing the center of each forest plot (resolution of 500m). Using the daily MODIS 2-band Enhanced Vegetation Index data (EVI2), the product yields the timing of phenometrics (vegetation phenology) over each year, including timing of greenup, midgreenup, peak, and senescence as used in this study. Data points were included in the analysis if they were flagged as "good" or "best" quality.

#### Weather data:

Climate data corresponding to the measurement periods were obtained from local weather stations at each focal site. For SCBI, weather data were obtained from a meteorological tower adjacent to the ForestGEO plot, via the ForestGEO Climate Data Portal v1.0 (<https://forestgeo.github.io/Climate/>). The R package climpact (see [www.climpact-sci.org](http://www.climpact-sci.org)) was used to plot temperatures for visual inspection and to identify readings that were >3 standard deviations away from yearly means, which were labeled as outliers and removed from the dataset. Gaps in the SCBI meteorological tower data were subsequently filled using temperature readings obtained from a National Center for Environmental Information (NCEI) weather station located in Front Royal, Virginia (<https://www.ncdc.noaa.gov/cdo-web/datasets/GHCND/stations/GHCND:USC00443229/detail>). Daily temperature records for Harvard Forest, which had already been gap-filled based on other local records, were obtained from the Harvard Forest weather station. For each site, we used records of daily maximum (T\_max) and minimum temperatures (T\_min).

Standardized Precipitation Evapotranspiration Index (SPEI) values were obtained from the ForestGEO Climate Data Portal v1.0 (<https://forestgeo.github.io/Climate/>).

#### Tree cores:

All tree cores had been previously collected, cross-dated, and measured using standard collection and processing methodologies. Details are provided in the original publications cited in the manuscript. For those chronologies not in previous publications, all tree cores were collected, processed, and analyzed with the same methods as those in the cited publications.

### Timing and spatial scale

Dendrometer band measurements were collected with no interruption in collection from 2011-2020 at SCBI and from 1998-2003 at Harvard Forest. Bands were measured with a digital caliper approximately every 1-2 weeks within the growing season. This sampling frequency was designed to capture the seasonality of stem growth. Measurements were timed to begin before the beginning of spring growth and to continue through the cessation of growth in the fall. At SCBI, the median start date was April 14, which was adjusted forward when early leaf-out of understory vegetation was observed, with the earliest start date being March 30 (in 2020). Measurements were continued through to fall leaf senescence, with the median end date being October 17 and the latest end date November 26 (2012). At Harvard Forest, all measurements from 1998 were dropped because of a late start date (May 26). Among the remaining years, the median start date was April 21 and median end date of October 27. 1999 was an anomalous year where initial measurements were taken on January 5, but not taken again until April 15. The latest end date was November 11, 2002.

Tree-ring chronologies were developed for 108 sites across the eastern North America, with analyzed years spanning from 1901-2019. Chronology end dates ranged from 1997 - 2019. The majority extended back prior to 1901, which was the first year analyzed due to climate data constraints.

#### Data exclusions

##### Dendrometer bands:

Data exclusions were planned to remove erroneous measurements of dendrometer bands or those that were unable to be modeled.

The raw dendrometer band data were screened before analysis to remove records or entire tree-years that were either unreliable or inappropriate for our analysis. First, we manually screened the data for three classes of errors. First, when a measurement was drastically different from previous and following measurements, it was assumed to be a human error and removed. Second, when measurements remained essentially unchanged for several readings, followed by a sudden jump then return to a normal growth pattern, this was assumed to be a case where the band was stuck on the tree bark and then released. In these cases, the full annual record for the tree was removed. Third, data points that deviated substantially from normal growth patterns, but for unknown causes, were removed. If a majority of the data points fell into this class within a tree-year, the entire year was removed from the analysis. We also removed tree-years with small or negligible total growth ( $\Delta\text{DBH} \leq 0.005 \text{ cm}$ ; SCBI = 26, Harvard Forest = 253), and tree-years where first intraannual measurement was later than the first spring survey (trees that were missed in the initial census; SCBI = 22, Harvard Forest = 8). These were removed because they reduce the reliability of predicted growth in the modeled curves.

After fitting the growth model, we removed tree-years with poor fits. Models were judged to be poorly fit if modeled growth parameters were outliers, which were commonly indicative of unrealistic fits (e.g., growth occurring outside the growing season or over a very short period) and underlain by very slow tree growth or poor data records that passed the initial screening (described above). Modeled fits for tree-years were removed under two conditions: (1)  $g_{\max}$  was  $\geq 2.5$  standard deviations away from the mean for each site-xylem architecture group combination (SCBI = 3, Harvard Forest = 11); (2) timing variables (DOY\_ip, DOY\_25, DOY\_50, DOY\_75) were  $\geq 2.5$  standard deviations away from the means for their site, xylem architecture group, and year (SCBI = 74, Harvard Forest = 101). At both sites the tree-years removed through this method were proportional to the original sample size, indicating that no species or size class was disproportionately removed compared to others. This process was repeated using 2 and 3 standard deviations as the cutoff for defining outliers, yielding qualitatively similar results.

##### Tree cores:

We did not exclude any tree-ring chronologies from the available set. Early years of chronologies were excluded if the subsample signal strength (SSS) was below 0.8. This follows established dendrochronological practices (e.g., Helcoski et al. 2018), wherein chronology start years are defined to ensure that a dominant proportion of the population signal (here,  $\geq 80\%$ ) was captured in the chronology.

#### Reproducibility

The study is not based on experiments.

#### Randomization

At SCBI, dendrometer bands were placed on a stratified random sample of trees within a the 25.6 ha ForestGEO plot, with additional trees from two 15-m radius plots in which all trees were sampled. Similarly, trees were cored on a stratified random sample of trees within the plot, and were also collected from all trees found dead in mortality censuses of 2015 and 2016.

At Harvard Forest, dendrometer bands were placed on trees within 36 circular, 10-m radius plots located randomly along eight 500-m transects that extended from the EMS eddy-flux tower. Similarly, tree cores were taken on all trees in nested circular plots (detailed in Dye et al. 2016; <https://doi.org/10.1002/ecs2.1454>).

Outside our focal sites, tree cores were collected either from canopy trees of the target species (traditional sampling approach, used for majority of chronologies) or from trees above a certain diameter (typically 10 cm DBH) within a censused plot. For chronologies sampled using a traditional approach, sampling targeted trees (typically  $>20$  individuals per site) of large size, in dominant canopy positions, and appearing old in age. This was not a randomized design, but rather targeted the individuals likely to display the most pronounced responses to climatic variation. For plot-based sampling, all trees above the selected diameter threshold within a defined plot were sampled. Methods for tree selection may influence the strength of observed climate signals, but are unlikely to influence the direction or seasonal patterns. In both cases, sampling captures the dominant trees that contribute most to forest productivity.

#### Blinding

Blinding was not necessary as we did not perform experiments containing treatments or groups, but rather analyzed long-term data records. The risk that human behavior could have introduced bias into data collection was minimal, given that the vast majority of dendrometer band data had already been collected, and tree-ring records collected and cross-dated, prior to formulation of the research question in spring/summer 2020.

Did the study involve field work?  Yes  No

## Field work, collection and transport

#### Field conditions

The study included 108 sites in eastern North America spanning 34.36 - 45.56°N latitude and 70.69 - 92.2°W longitude. Focal sites, where dendrometer bands were measured, included the Smithsonian Conservation Biology Institute (SCBI) ForestGEO plot (38.8935° N, 78.1454° W; 25.6 ha; elevation 273–338 m.a.s.l.) and the Harvard Forest ForestGEO plot (42.5388° N, 72.1755° W; 35 ha; 340–368 m.a.s.l.).

At SCBI, the climate is humid temperate, with 1950-2019 mean annual precipitation of 1018 mm and temperatures averaging 1°C in January and 24°C in July. Within the study period for the dendrometer band analysis (2011-2019), spring temperatures (March and April Tmax; source: CRU v.4.0454) and summer Standardized Precipitation Evapotranspiration Index (SPEI) values (4-month value of August) were similar to the average climate prior to the study period (1970-2010). Specifically, average spring Tmax was  $16.9 \pm 1.4^\circ\text{C}$  (mean  $\pm$  1SD) prior to the study period (range: 14.1-19.9) and  $17.6 \pm 1.7^\circ\text{C}$  (range: 15.6-20) during the study period, while summer

SPEI was  $-0.06 \pm 1.02$  (range: -1.7-2.4) prior to the study period and  $0.5 \pm 0.8$  (range: -0.8-1.6) during.

At Harvard Forest, the climate is temperate continental, with 1950-2019 mean annual precipitation of 1104 mm and temperatures averaging  $-5^\circ\text{C}$  in January and  $22^\circ\text{C}$  in July. Within the study period for the dendrometer band analysis (1999-2003), spring temperatures (March and April Tmax; source: CRU v.4.0454) and summer SPEI values (4-month value of August) were similar to the average climate prior to the study period (1970-1998). Specifically, average spring Tmax was  $10.9 \pm 1.5^\circ\text{C}$  prior to the study period (range: 8.0-13.2) and  $11.2 \pm 1.0^\circ\text{C}$  (range: 10.1-12.2) during the study period, while summer SPEI was  $0.1 \pm 0.9$  (range: -1.8-1.7) prior to the study period and  $0.2 \pm 0.9$  (range: -1.0-1.1) during. The driest summer during the study period (1999) had the 5th lowest SPEI value (-1.0) in the period 1970-2003, with precipitation of 52 mm mo<sup>-1</sup> in June-August compared to average monthly precipitation of 100+ mm<sup>35</sup>.

Dendrometer band measurements were made during the growing season from spring to autumn. Weather conditions have a modest effect on these readings. For example, stems shrink and swell depending upon hydration status (which, in turn, is affected by soil moisture and vapor pressure deficit), and metal bands may be modestly affected by temperatures (through thermal expansion of metal). These effects should be largely removed through the fitting of a seasonal growth model (detailed in methods section) and are not expected to bias our analysis.

Tree cores were collected at various times of the year. Weather conditions at the time of collection would have no effect on these readings.

#### Location

Smithsonian Conservation Biology Institute (SCBI) ForestGEO plot ( $38.8935^\circ\text{N}, 78.1454^\circ\text{W}$ ; 25.6 ha; elevation 273–338 m.a.s.l.)  
Harvard Forest ForestGEO plot ( $42.5388^\circ\text{N}, 72.1755^\circ\text{W}$ ; 35 ha; 340-368 m.a.s.l.)  
106 additional sites spanning the eastern North America (locations listed in Supplementary Information)

#### Access & import/export

Site access and sampling at SCBI and Harvard Forest was conducted under the permission and following the guidelines of these institutions. For tree core sampling at the 106 non-focal sites, all site access and sample collection was done with permission from the appropriate authorities. There was no import/export of samples across international borders.

#### Disturbance

Disturbance to the forests from which we collected samples was minimized to the best of our abilities by always adhering to leave no trace practices.

Dendrometer bands were installed over the surface of tree bark and have no known impacts on tree health.

Tree cores (5-mm diameter) were extracted from sampled trees. An analysis conducted at SCBI revealed that coring had no detectable effect on tree mortality (Helcoski et al. 2018, Tree-Ring Research).

## Reporting for specific materials, systems and methods

We require information from authors about some types of materials, experimental systems and methods used in many studies. Here, indicate whether each material, system or method listed is relevant to your study. If you are not sure if a list item applies to your research, read the appropriate section before selecting a response.

### Materials & experimental systems

- |                                     |  |
|-------------------------------------|--|
| n/a                                 | Involved in the study                                  |
| <input checked="" type="checkbox"/> | <input type="checkbox"/> Antibodies                    |
| <input checked="" type="checkbox"/> | <input type="checkbox"/> Eukaryotic cell lines         |
| <input checked="" type="checkbox"/> | <input type="checkbox"/> Palaeontology and archaeology |
| <input checked="" type="checkbox"/> | <input type="checkbox"/> Animals and other organisms   |
| <input checked="" type="checkbox"/> | <input type="checkbox"/> Human research participants   |
| <input checked="" type="checkbox"/> | <input type="checkbox"/> Clinical data                 |
| <input checked="" type="checkbox"/> | <input type="checkbox"/> Dual use research of concern  |

### Methods

- |                                     |   |
|-------------------------------------|---|
| n/a                                 | Involved in the study                           |
| <input checked="" type="checkbox"/> | <input type="checkbox"/> ChIP-seq               |
| <input checked="" type="checkbox"/> | <input type="checkbox"/> Flow cytometry         |
| <input checked="" type="checkbox"/> | <input type="checkbox"/> MRI-based neuroimaging |